Biogeosciences

Discussions

Nitrification in the oligotrophic Atlantic Ocean.

Darren R. Clark[1], Andrew P. Rees[1], Charissa Ferrera[2], Lisa Al-Moosawi[1], Paul J. Somerfield[1], Carolyn Harris[1], Graham D. Quartly[1], Stephen Goult[1], Glen Tarran[1], Gennadi Lessin[1].

[1]Plymouth Marine Laboratory, Prospect Place, The Hoe, PL1 3DH.

5   [2]The Marine Science Institute, Velasquez St., University of the Philippines, Diliman, Quezon City 1101 Philippines.

Correspondence to: Darren Clark (drcl@pml.ac.uk)

Abstract. The recycling of scarce nutrient resources in the sunlit open ocean is crucial to ecosystem function. Ammonium oxidation, the first stage of the nitrification process, directs ammonium derived from organic matter decomposition towards the regeneration nitrate, an important resource for photosynthetic primary producers. However,
10   the technical challenge of making nitrification rate measurements in oligotrophic conditions combined with the remote nature of these marine systems means that data availability, and the understanding that provides, is limited. This study reports rate measurements of ammonium oxidation over a 13, 000 km transect within the photic zone of the Atlantic Ocean. These measurements, at relatively fine resolution (order 300 km), permit the examination of interactions with environmental conditions that may warrant explicit development and inclusion in model descriptions. At all locations
15   we report measurable rates with significant variability between and within Atlantic provinces. This adds to evidence that nitrification is an important component of pelagic nitrogen cycling which modifies the inorganic nitrogen inventory of the sunlit ocean. Particular features of interest included a significant hemispheric difference in ammonium oxidation rate and elevated rates associated with mesoscale eddy features. Statistical analysis of potential links between ammonium oxidation rate and routinely measured ecosystem variables indicated significant correlative structure,
20   explaining ~65% of the data variability. Differences between sampling depths were of the same magnitude or greater than horizontally resolved differences along the transect length, identifying distinct biogeochemical niches between depth horizons. Principle component analysis demonstrated that the best overall match between ammonium oxidation rate and environmental variables involved a combination of chlorophyll-a concentration, the duration of the light phase and silicate concentration (which we argue to be a short-term tracer of physical instability). Results allude to an
25   association between ammonium oxidation and potentially short-term product(s) of photosynthetic activity and subsequent degradation. Approximately 35% of data variability was not explained, which may include descriptions of DOM pool dynamics.

1 Introduction

Oligotrophic gyres and their transition regions are the largest biome on Earth, covering approximately 60% of its
30   surface (Eppley and Peterson, 1979), and are expanding as a result of the warming climate (Polovina et al., 2008). Biogeochemical processes in these regions have the potential to influence global elemental cycles. Within the sunlit ocean, photosynthetic cells fix carbon dioxide (CO_2) and assimilate inorganic nutrients to synthesise organic molecules and build biomass (Azam et al., 1983). Either directly or indirectly, this biomass supports the ecosystem and contributes over half of global organic carbon export (Emerson et al., 2001). Persistent stratification in these systems impedes
35   nutrient inputs to the sunlit region from the deep ocean, constraining microbial growth (Eppley and Peterson, 1979, Moore et al., 2013). Consequently, efficient organic matter decomposition and inorganic nutrient regeneration are crucial to ecosystem function. Decomposition regenerates inorganic nitrogen in the form of ammonium (NH_4^+), which rarely accumulates in the open surface-ocean as it is readily used in anabolic and chemotrophic microbial processes. Evidence demonstrates that nitrification, the 2-stage oxidation of NH_4^+ via nitrite (NO_2^-) to nitrate (NO_3^-), takes place in
40   the photic zone of open oceans (Santoro et al., 2013) where it directly competes with photosynthetic cells for the NH_4^+ resource (Smith et al., 2014). The outcome of this competitive interaction is important; by moderating the composition and concentration of the dissolved inorganic nitrogen pool (NH_4^+, NO_2^-, NO_3^-), nitrification influences nutrient limitation patterns for primary production at the basin scale (Partensky et al., 1999; Palinska et al., 2002; Fawcett et al., 2015; Moore et al., 2013). Biological processes within the ocean's upper mixed layer modify its chemistry and
45   subsequently influence the composition of deep water masses through particle sedimentation, decomposition and remineralisation, with global implications for productivity and climate over a range of temporal scales (Rafter et al.,

Biogeosciences
Discussions
EGU
Open Access

2013; Tuerena et al., 2015). In addition, nitrification is a source of the climatically active gas N_2O within the surface ocean, which readily exchanges with the lower atmosphere. The yield of N_2O from nitrification is the cause of greatest uncertainty in global oceanic N_2O emission budgets (Santoro et al., 2011; Zamora and Oschlies, 2014). Characterising
50 the distribution and constraints on nitrification is an important step towards fully assessing pelagic nitrogen transformations in the open ocean, although observations at the oceanic basin scale are limited (Clark et al., 2008; Shiozaki et al., 2016).

Within the open oceans, pelagic nitrification is distributed in a characteristic depth profile; low rates are measured in the well-lit near-surface waters while the highest rates are reported at, or close to, the base of the well-lit photic zone in
55 association with the primary nitrite maximum (PNM) and the deep chlorophyll maximum (DCM); rates drop rapidly below this depth into the twilight zone of the mesopelagic (Smith et al., 2016; Newell et al., 2013). Observational data have been crucial to the development of this understanding and indicate that environmental factors act simultaneously to structure the vertical distribution of nitrifying organisms and their activity. Evidence identifies roles for light, NH_4^+ concentration, organic matter flux and competitive interactions with phytoplankton (Fawcett et al., 2015; Shiozaki et al.,
60 2016; Olson, 1981; Smith et al., 2014; 2016; Bresseler and Boyd, 2009; Newell et al., 2011). However, the statistical analysis of nitrifying organism activity and diversity in relation to environmental factors explains only a fraction of the data variability, alluding to further complex and undefined interactions between the nitrifying activity of these organisms and their environment (Clark et al., 2014; Bouskill et al., 2012). A better appreciation of the factors that most significantly influence nitrifying activity is required to guide future fieldwork observations and ultimately, the
65 development and explicit inclusion of such relationships in models.

Here we present relatively high-resolution photic zone measurements of the first stage of nitrification – ammonium oxidation rate (R_{NO2}) - across a 13,000 km oligotrophic Atlantic Ocean transect to examine the process rate distribution and potential links to environmental conditions. Investigations were conducted during the Atlantic Meridional Transect program (Rees et al., 2017), which, since 1995, has undertaken annual (or bi-annual) scientific observations of the
70 Atlantic Ocean between the UK and southern hemisphere locations including the Falkland Islands and Punta Arenas (Chile). The cruise track has historically navigated through marine provinces that include the Atlantic gyres, the equatorial upwelling convergence zone, mesotrophic fringing regions and regions influenced by eastern boundary upwelling ecosystems (Mauritania, Benguela), sampling significant variability in biological, physical and chemical conditions. By navigating between hemispheres, observations incorporate contrasting seasons, a signature that is
75 evident in biogeochemical observations, despite persistent water-column stability that typifies tropical and sub-tropical open oceans. Within this observational context, the overarching objective of the study was to highlight interactions between the rate of ammonium oxidation and environmental conditions that may warrant explicit development and inclusion in model descriptions.

2. Methods

80 ### 2.1 Water column characterization.

This study was undertaken during the Atlantic Meridional Transect (AMT) cruise 19 (13th October to 1st December 2009) aboard the RRS James Cook between Falmouth (UK) and Punta Arenas (Chile; Fig. 1), passing through the following Atlantic provinces (Longhurst, 1998); North Atlantic Drift (NADR), North Atlantic subtropical gyre (NAST), North Atlantic tropical gyre (NATR), Western tropical Atlantic (WTRA), South Atlantic gyre (SATL). Seawater was
85 collected for biogeochemical observations from a total of 120 CTD-rosette casts, of which 33 were used for isotope studies to derive rates of ammonium oxidation. An instrumental package was deployed during solar noon to derive light depth profiles using Photosynthetically Active Radiation (PAR) data recorded by a Chelsea Instruments PAR sensor. A stainless-steel rosette unit was deployed during dawn casts (typically 06:00 GMT), incorporating a Sea-Bird 9/11 plus Conductivity, Temperature, Depth system, a Chelsea MKIII Aquatracka fluorimeter and 20 L Niskin bottles for water
90 collection from specific sampling depths.

2.2 Nutrient analysis.

Inorganic nutrient samples collected from dawn casts were immediately analysed. Nitrite (NO_2^-), nitrate (NO_3^-), phosphate (PO_4^{3-}) and silicate ($Si(OH)_4$) were measured colorimetrically with a 5-channel segmented flow Bran and

Luebbe AAIII autoanalyzer, using methods described previously (Woodward and Rees, 2001). The concentration of
95   NH_4^+ was not determined during this study.

2.3 Analytical Flow Cytometry.

Microbial cells were enumerated based on their light scattering and auto-fluorescence properties using a BD
FACSort™ flow cytometer. Photosynthetic cells were analysed live within 1-2 hours of collection. Non-photosynthetic
cells were fixed with paraformaldehyde for 1 hour at 4 °C and then stained with SYBR Green I DNA stain (Life
100   Technologies, Paisley, UK) in the dark at room temperature for 1 hour. Live samples were analysed at a flow rate of
180 μL min^{-1} for 4 minutes. Fixed/stained samples were analysed at either 50 or 12 μL min^{-1} for 1-2 minutes, depending
on concentration. Data acquisition for photosynthetic cells was triggered on red (chlorophyll) fluorescence while the
enumeration of SYBR Green I-stained bacteria and archaea was triggered on green fluorescence. Flow rates were
calibrated daily using fluorospheres of known concentration.

105   **2.4 R_{NO2} determination using ^{15}N isotope studies.**

Approximately 4 L of seawater collected from depths equivalent to 14 %, 1 % and 0.1 % of surface measured PAR
(sPAR) was used for R_{NO2} studies. The isotope dilution approach (Clark et al., 2007; 2008; 2014) was used to derive the
rate of ammonium oxidation, by measuring the rate of product formation (NO_2^- regeneration). These 4 L sample
volumes were amended with $^{15}NO_2^-$ at < 10 % of the ambient concentration. Following amendment, triplicate 500 mL
110   sub-samples were taken. Within these triplicate sub-samples, pre-incubation NO_2 concentration and ^{15}N enrichment was
determined by synthesising Sudan-1 (see below) from sample NO_2^-. Sudan-1 is synthesised for this purpose as it is
readily formed and collected at room temperature, it is stable and amenable to both purification and isotopic analysis.
From the remaining volume, triplicate 500 mL incubation vessels were filled and placed in deck incubation units
covered with neutral density filters to simulate sPAR depths according to Joint Global Ocean Flux Study protocols
115   (IOC, 1994). Incubation boxes were flushed with recirculating depth-appropriate temperature-controlled seawater.
Following approximately 10 hours of day-time incubation, experiments were terminated by GF/F filtration. Sudan-1
was synthesised from NO_2^- within 500 mL samples, allowing post-incubation NO_2^- concentration and ^{15}N enrichment to
be measured. During these studies, a pre-incubation $^{15}NO_2^-$ enrichment of 5.41±2.18 % was achieved, which was
diluted by 0.92±0.83 % on average due to biological activity during incubation.

120   For the synthesis of Sudan-1, the first reagent (0.8 g of aniline sulphate in 200 mL 3 M HCl) was added to samples
in the proportion 0.5 mL per 100 mL sample volume. After mixing, samples were left for 5 minutes to homogenize,
after which sample pH was verified to be approximately 2.0. Reagent 2 (24 g NaOH and 0.416 g 2-napthol in 200 mL
Milli Q) was added in the proportion 0.5 mL per 100 mL sample volume. Samples were again mixed and left for 5
minutes before sample pH was verified to be approximately 8.0. The development of Sudan-1 was complete after 30
125   minutes of incubation at room temperature. Samples were acidified with citric acid (final pH 5.5) and an appropriate
volume of deuterated Sudan-1 internal standard (100 ng·μL^{-1}) was added. Deuterated Sudan-1, which was used for
sample quantification, was synthesized and purified according to methods described previously (Clark et al., 2006;
2007). Samples were collected by solid phase extraction (SPE) using octadecyl (C18) 6 mL, 500 mg cartridges. SPE
columns were stored at -20 °C until analysis.

130   At the land-based laboratory, samples eluted from SPE cartridges were purified by high performance liquid
chromatography (HPLC). Using a ramping methanol/Milli-Q water profile in combination with a Gemini-NX 5u C18
110A 250×4.6 mm column, sample peaks were resolved. The peak containing Sudan-1 internal standard was retained
using a fraction collector while the remaining sample volume was discarded. Fraction-collected samples were dried and
stored over anhydrous silica gel until further analysis.

135   Purified silylated samples were analysed by Gas Chromatography Mass Spectrometry using a HP-5ms column (30
m x 0.25 mm internal diameter), with the ramping profiles and extracted ions described in Clark et al. (2007). Using
NO_2^- concentration and enrichment measurements, the rate of NO_2^- dilution was determined by applying the Blackburn–
Caperon model (Blackburn, 1979; Caperon et al., 1979).

2.5 Statistical analysis.

4

140   R_{NO2} rate data and associated explanatory variables were analysed using a range of multivariate statistical methods (Clarke et al., 2014). Most variables were skewed, so prior to analysis all variables except phosphate excess (P*; calculated as $P*=[PO_4^{3-}]-([NO_3^-]/16)$) were log-transformed to reduce the influence of extreme values in subsequent analyses. Variables were normalized by subtracting the mean and dividing by the standard deviation to convert them all to a common dimensionless scale. Relationships among samples based on the explanatory variables were visualised

145   using Principal Components Analysis (PCA), and hypothesis testing for differences among groups of samples was undertaken using Analysis of Similarities (ANOSIM) with ordered factors (Somerfield et al., 2021). The generalised ANOSIM statistic is a scaled measure of effect size comparable across different tests.

       To analyse relationships between R_{NO2} rates and explanatory variables the data for each sPAR band were analysed separately. To determine whether there was structure among variables that warranted further analysis, explanatory

150   variables were subject to Type 2 Similarities Profiles (SIMPROF) analysis (Somerfield and Clarke, 2013). A Euclidean distance matrix was calculated for R_{NO2} rates. A stepwise search algorithm (BVSTEP) with forward selection and backward elimination steps (Clarke and Warwick, 1998) was used to search for the smallest subset of explanatory variables that, in combination, 'best matched' the pattern of R_{NO2} rates across samples, the best match being defined as maximising the rank correlation between corresponding distance matrices. The algorithm was run with 20 restarts of 6

155   randomly selected variables. The significance of the maximum rank correlation was tested using an appropriate permutation test (Clarke et al., 2008).

2.6 Contemporaneous physical oceanography data.

       The ship, RRS James Cook made routine physical measurements whilst underway using the thermosalinograph to give temperature and salinity of the water at ~5m depth, and a depth profile of currents relative to the ship using the

160   vessel-mounted 150 kHz Acoustic Doppler Current Profiler (ADCP). The latter were corrected using the ship's navigation to give absolute instantaneous currents along the ship's track. To put these measurements in context, data were subsequently obtained from satellite altimeter and profiling floats that were in the area. These two sources of data were particularly useful in understanding anomalous observations at two of the CTD stations (28 °S, 39 °S).

       The altimetry data were sourced from Copernicus Marine Environment Monitoring Service (CMEMS) who combine

165   the sea surface height measurements from available observations and interpolated these data on to a regular 0.25° x 0.25° grid. Variations in sea level at the mesoscale (order 100-300 km) could be interpreted as eddies, with a local negative anomaly having cyclonic flow about it (clockwise in the southern hemisphere) and highs (anticyclones) having flow in the opposite direction. These flows were in geostrophic balance and thus represent stable current regimes, not incorporating tides or the effect of short wind bursts. Because of the long and near global altimetric record these data

170   can be used to identify regions of persistent variability and to track the evolution of features over periods ranging from weeks to years. However, satellites only give a near-surface view.

       Profiles of temperature and salinity in the vicinity of the ship's track were provided by Argo floats, which are autonomous profilers typically recording 0-2000 m vertical sections every 10 days. As these instruments are freely drifting within the ocean, the location and timing of their measurements are not linked to that of the ship. Argo data for

175   the required regions were obtained, and the profiles analysed to give a measure of the Mixed Layer Depth (MLD) as the depth at which temperature was more than 3 °C below that of the surface.

3. Results

3.1 Temperature, salinity and PAR.

       Characteristic physical features of oligotrophic oceans were demonstrated (Fig. 2a, b, c). The water column was

180   thermally stratified, with sampling locations straddling a temperature range of approximately 12-29 °C. The deepest mixed layer depths were associated with the central regions of the Atlantic gyres. Stratification weakened towards the northern and southern limits of the transect. In terms of salinity, sampling depths incorporated a range of 34.3-37.5. The most saline regions were associated with the ocean gyres and were highest in the Northern gyre. A region of relatively low salinity water was associated with the surface 30 m of the WTRA, defining the lower limit of the salinity range

185   measured. In terms of the light field, 0.1% sPAR defined the deepest sampling point and equated to a depth within the range 75-200 m. Light dose (defined as the light intensity multiplied by the day-light duration) across sampling depths

spanned ~2 orders of magnitude. Day light duration increased progressively south, associated with the seasonal transition from boreal autumn to austral spring.

3.2 Inorganic nutrients and dissolved oxygen.

190   Inorganic nutrient concentration measurements (Fig. 3) demonstrated oligotrophic (< 100 nmol L^{-1} NO_3^- and PO_4^{3-}) conditions throughout the transect at 14 % sPAR. At the 1 % sPAR depth, the concentration of NO_3^- and PO_4^{3-} was generally low (<600 nmol L^{-1} and <150 nmol L^{-1} respectively). The highest concentrations of NO_3^- and PO_4^{3-} were measured at the 0.1 % sPAR depth, notably in the NATR/WTRA/SATL region. A P* of approximately 0.2 µmol L^{-1} was measured at South Atlantic stations. A NO_2^- concentration maximum was associated with the 1 % sPAR depth
195   where an average of 117±112 nmol L^{-1} was measured. Extremely low concentrations of $Si(OH)_4$ were measured in the well-lit surface ocean, progressively increasing at 1% and 0.1 % sPAR depths.

        The dissolved oxygen concentration was generally within the range 200-280 µmol L^{-1}, with the exception of the 0.1 % sPAR depth in the NATR/WTRA/northern SATL, where concentrations approaching 100 µmol L^{-1} were measured.

200   Plots of dissolved oxygen concentration against salinity (a), temperature (b) and NO_3^- (c) are presented in Fig. 4. Low dissolved oxygen concentrations measured at 0.1 % sPAR within NATR/WTRA/SATL provinces were associated with lower salinity, temperature, and relatively high NO_3^-. R_{NO2} measurements associated with low-oxygen sampling depths were not anomalously elevated (Fig. 4d). In contrast, the R_{NO2} rate and physio-chemical characteristics of the eddy station identified as 39 °S distinguished it from the conditions associated with the majority of sampling stations
205   within the transect.

3.3. Microbial cell distribution and abundance.

        Profiles of chlorophyll-a concentration (Fig. 5a) indicated that within provinces of the North Atlantic, the sub-surface maximum generally deepened progressively south. The highest chlorophyll-a concentration was measured within the WTRA, although there was considerable variability in the depth of the chlorophyll-a maximum within this
210   province. Within the South Atlantic, although sampling stations were classified as SATL province, chlorophyll-a profiles could be grouped into four illustrative sub-divisions, characterised by a general shallowing of the chlorophyll-a maximum progressively south.

        Pico-eukaryotes (Fig. 5b) had a distribution that was similar to that of chlorophyll-a, in contrast to the profiles of the photosynthetic cyanobacteria *Synechococcus* and *Prochlorococus* (results not shown). Bacterial cell distribution (Fig.
215   5c) was comparable between gyres, though less defined within the WTRA, and indicated that the highest bacterial abundance was measured within the relatively well-lit surface ocean.

3.4. Rates of R_{NO2}

        Within the physical, chemical and biological context described above, rates of ammonium oxidation were measured (Fig. 6). For all R_{NO2} data (Fig. 7a-c), the range of volumetric rate measurements was 0.02-13.27 nmol-N L^{-1} d^{-1}, n=88
220   triplicated measurements. When integrated from the surface to the 0.1% sPAR, the range of R_{NO2} was 0.01-0.91 mmol N m^{-2} d^{-1}. By extrapolating the vertically integrated results of each station (excluding 28°S and 39°S) from the equator into each hemisphere across a comparable distance (Fig. 8), the concentration of ammonium-N oxidised was calculated to be 0.36 mol N d^{-1} (1 x 4457 km transect) and 0.72 mol N d^{-1} (1 x 4637 km transect) for the NAG and SAG respectively. The box plot presented in Fig. 7(d) highlights variability within discrete sPAR bands of each hemisphere
225   with mean R_{NO2} values generally skewed towards the lower region of the data range. The distribution of rate measurements is presented in Fig. 7(e) while provincial variability, which averaged 25-fold, is presented in Fig. 7(f). Using a 2 sample t-test assuming unequal variance, R_{NO2} at 1% sPAR in the North Atlantic (M=0.76 nmol L^{-1} d^{-1}, SD=0.67 nmol L^{-1} d^{-1}) was significantly lower than R_{NO2} at 1% sPAR in the South Atlantic (M=1.77 nmol L^{-1} d^{-1}, SD=1.52 nmol L^{-1} d^{-1}); t(15)=-2.40, p=0.03 (no significant difference between hemispheres was found for 14% and 1%-
230   50m sPAR depths). Volumetric rates of R_{NO2} equated to a NO_2 turnover of 0.4-335 days (average 33 days).

3.5 Multivariate analysis.

Principle Component Analysis (PCA) of the full set of 24 environmental variables considered (Table 1; Fig. 9) clearly demonstrated that differences between sPAR bands were of the same magnitude or greater than differences along the transect length. PC1, separating the sPAR bands, explained 42.7% of the total variation while PC2,

235 representing latitudinal variation, explained 23.4%. This was supported by 2-way ANOSIM with ordered factors, latitude and sPAR band, where the test for differences among latitudes removing differences over sPAR bands (R^O=0.465, p<0.001) gave a lower value for the statistic than the corresponding test for differences among sPAR bands removing latitudinal trends (R^O=1, the maximum possible, p<0.001). It was thus decided to analyse relationships among R_{NO2} rates and environmental variables within each sPAR band separately.

240 Type 2 similarity profiles (SIMPROF) showed evidence for significant correlation structure among variables in all 3 sPAR bands (14% sPAR band, π=0.296, p<0.001; 1% sPAR band, π=0.205, p<0.001; 0.1% sPAR band, π=0.157, p<0.001). In the 14% sPAR band there was a significant relationship (ρ=0.313, p=0.025) between patterns in R_{NO2} rates and a subset of 3 explanatory variables consisting of light hours, chlorophyll-a and silicate. In the 1% sPAR band the best subset, also of 3 variables, contained light hours and chlorophyll-a, but with NO_2 instead of silicate. The overall

245 relationship was not significant (ρ=0.170, p=0.474). In the 0.1 % sPAR band the best subset (ρ=0.415, p<0.001) contained 6 variables, light hours and chlorophyll-a, temperature, NO_2^-, PO_4^{3-} and P*. A 2-way search for the best overall match within sPAR bands removing any latitudinal effect selected light hours, chlorophyll-a and silicate, ρ_{ave}=0.267, p<0.001.

3.6 Eddy features 28 °S and 39 °S.

250 The majority of the AMT transect ran through quiescent waters free from rapidly varying mesoscale features. The equatorial belt is a region of counter-flowing currents, but these did not lead to any unusual features during this particular AMT campaign. However, anomalous profiles were observed at 28 °S and 39 °S (Fig.1), in the form of conspicuously prominent R_{NO2} rates (Fig. 7a-c). The spatial separation of CTD stations (~300 km) was too great to resolve these physical features. Thus, altimeter and Argo data were obtained subsequent to the cruise in order to provide

255 context to these observations.

Mapped fields of Sea Surface Height (SSH) from CMEMS were used to calculate the mean sea surface topography and the variations about that. A map of the root mean square variability (Fig. 10c) demonstrated that the typical changes north of 35 °S to be only ~0.1 m; however, even in this region there were a number of highs in the SSH anomaly (deviation from the mean) at the time of sampling the 28 °S station (Fig. 10a). The anticyclonic feature centred on

260 station 28 ^{0}S had anticlockwise geostrophic flow along the contours in SSHA, whilst the total near-surface velocity recorded by the ADCP was mainly to the southwest. A series of SSHA composites a week apart showed a central anticyclonic feature to be moving westwards, whilst the contemporaneous Argo profiles showed that the thickest mixed layer was located close to the centre of this feature (Fig. 10b). A larger anticyclonic feature was seen 400 km further to the east. Examination of a time series of SSHA maps and Hovmöller diagrams (not shown) confirmed that these

265 features had travelled from the Agulhas Retroflection, taking 2.5 years to get to this location.

The feature around CTD station 39 °S was very different. This is the region of the Brazil-Falklands Confluence, where two strong currents collide generating significant mesoscale activity and locally generated eddies. These features also move westwards, but their associated water masses were not from the Agulhas region. In this region the total velocities from the ADCP agreed with the contour directions governing the geostrophic flow. As it is a much more

270 active region, Argo floats do not remain in the region for long, so the examples found (Fig. 10d) were more dispersed than in the previous case. Using the previously stated definition of MLD produced much larger values than at 28 °S, but again supported the concept that the surface layer was much deeper over the highs in SSH than over the lows.

4 Discussion

4.1 Overview and objectives.

275 This study measured rates of ammonium oxidation within the photic zone across an extended spatial scale (13,000 km), reporting significant variability between and within provinces of the oligotrophic Atlantic Ocean between ~49 °N and ~39 °S. Insights add to evidence that surface ocean nitrification is an important component of pelagic nitrogen cycling that modifies the inorganic nitrogen inventory. Particular features of interest included a significant

hemispheric difference in ammonium oxidation and elevated rates associated with mesoscale eddy features. Analysis of
280 potential links between ammonium oxidation and routinely measured ecosystem variables indicated significant co-
variability between ammonium oxidation, chlorophyll-a concentration, the duration of the light phase and silicate
concentration, alluding to an association between ammonium oxidation and product(s) of photosynthetic activity.
However, a significant fraction (~35 %) of variability in ammonium oxidation remained unexplained, indicating that
additional factors were excluded from this analysis. We first consider the biogeochemical context to the study before
285 presenting rate observations and insights from statistical analysis.

4.2 Physical context

A thermal range of ~17 °C typically existed in vertical 250 m water column profiles. While temperature has a direct
impact on rates of biological activity, the physical stability of the water column caused by thermal stratification
establishes spatially distinct biogeochemical niches (Giovanoni and Vergin, 2012). Within the well-lit surface ocean
290 that includes the 14 % sPAR, defined as the region between the sea-surface and the deep chlorophyll-a maximum
(DCM), turbulent mixing with nutrient rich deep water is supressed and biological activity maintains extremely low
inorganic nutrient concentrations. Relatively sharp physio-chemical gradients at depths similar to the 1 % sPAR create a
niche where low light-adapted phototrophs access relatively high inorganic nutrient concentrations, forming the DCM.
At greater depths, incorporating the 0.1 % sPAR and typically referred to as the twilight zone (approximately 100-
295 1000 m), water continues to cool. While there is relatively little information for the temperature sensitivity of
nitrification in the open ocean, Horak et al., (2013) demonstrated a relative insensitivity to a temperature range of 8-
20 °C in their study of a fjord-like basin, although low pH at the study site may have constrained any temperature
response (Beman et al., 2011).

The range in salinity was ~3.2, with limits defined by notably fresher water in the sub-tropical region (WTRA), a
300 feature potentially related to intense rainfall within the inter-tropical convergence zone, and relatively high salinity in
the central Atlantic gyres. While a contributory role for salinity in shaping nitrifying community structure has been
identified in studies of estuarine sediments (Francis et al., 2003; Bernhard et al., 2010), such gradients are considerably
more extreme than those of the open oceans, where little, if any information is available to describe its influence upon
variability in nitrification rate.

305 The attenuation of light with depth leads to progressively decreasing daily light dose, ranging 2 orders of magnitude
across the three R_{NO2} sampling depths (Fig. 2c). Superimposed upon diel and depth-related light variability was a
seasonal increase in day-light duration progressively south, associated with the transition from boreal autumn to austral
spring. Seasonally variable characteristics are evident in the photic zone of sub-tropical Atlantic gyres driven by
changes in solar insolation (McClain et al., 2004). Weaker solar insolation during winter supresses DCM productivity,
310 allowing higher nutrient concentrations to pass this 'biological filter' into the well-lit surface ocean. This mechanism
supports higher chlorophyll-a concentrations in the surface ocean (Taylor et al., 1986) and would presumably stimulate
broader biological activity, including the decomposition of recently produced organic matter and the regeneration of
nutrients. Seasonality in the rate of nitrification was not evident in the study of Yool et al. (2007), although such a
signal may exist (Newell et al., 2013).

315 Evidence demonstrates that light structures the distribution of nitrifying organisms, whose activity may be supressed
within the photic zone (Shiozaki et al., 2016; Olson et al., 1981). Further, by poorly competing with photosynthetic
plankton for NH_4^+ resource, nitrifier distribution and activity is indirectly constrained by the light regime (Ward, 1985;
Smith et al., 2014). While the light/dark cycle may lead to a diel variability in nitrifying activity (increasing at night
with the recovery from light inhibition; Smith et al., 2014), resource competition with phytoplankton may persist due to
320 their capacity for dark N-assimilation, especially of NH_4^+ (Clark et al., 2002).

4.3 Chemical context

In terms of the chemical context to the study, characteristically low concentrations of NO_3^-, PO_4^{3-} and $Si(OH)_4$ were
evident within the well-lit surface ocean (14 % sPAR), progressively increasing at 1 % and 0.1 % sPAR (Fig. 3.a, b, f).
This distribution is consistent with biological draw-down, likely dominated by nutrient acquisition by phototrophs
325 (Poulton et al., 2006; Marañon et al., 2000). Extremely high concentrations were a prominent feature of nutrient profiles
within the deep equatorial region.

Biogeosciences
Discussions

8

In the mesopelagic ocean, nitrification maintains the accumulation of NO_3^-, while the diapycnal nutrient flux to the surface open ocean is relatively weak, especially during periods of low wind energy input. NO_3^- supplied via nitrification in the photic zone is either extremely low (Clark et al., 2008; Newell et al., 2013) or below detection
330 (Lomas et al., 2009). Alternative NO_3^- and PO_4^{3-} sources to the surface ocean includes introduction as a component of atmospheric dust (Gruber and Sarmiento, 1997; Baker and Jickells, 2017), subsurface injections via the action of internal tides over mid-ocean ridges (Tuerena et al., 2019) or the passage of mesoscale eddies (McGillicudy et al., 1998; Oschilies and Garcon, 1998). No direct correlation between nitrification and NO_3^- concentration has been reported. A relationship with PO_4^{3-} availability has been demonstrated in water treatment systems (de Vet et al., 2012), although
335 there is no evidence to support this correlation in low nutrient environments.

Analytical capacity for nano-molar NH_4^+ measurements was unavailable for this study, creating a potentially significant shortfall in the data set, since NH_4^+ concentration has been demonstrated to influence the activity, distribution and composition of nitrifying communities (Bouskill et al., 2012; Smith, 2016). As the primary resource for nitrification, it is intuitive to expect a direct relationship between ammonium oxidation rate and NH_4^+ concentration
340 (Smith et al., 2016), evidence for which supports the representation of this process as the specific rate (d^{-1}; Yool et al., 2007). However, this correlation is not consistently demonstrated (Bouskill et al., 2012) and the process of NH_4^+ oxidation may exhibit saturation kinetics (Shiozaki et al., 2016; Martens-Habbena et al., 2009).

A phosphate excess similar to 0.2 µmol L^{-1} was evident at all depths in the WTRA and SATL (Fig. 3c). This feature is related to both source waters (Sarmiento et al., 2004) and the interhemispheric difference in N-fixation, supported by
345 micro-nutrient inputs via atmospheric dust deposition (Baker and Jickells, 2017), leading to P* drawdown in the North Atlantic (Moore et al., 2009). There is no evidence of a direct relationship between P* and nitrification rate. However, in Atlantic regions of enhanced N-fixing activity, evidence suggests that organic material produced by diazotrophs is recycled within the surface ocean (Mulholland, 2007). While nitrification has rarely been measured simultaneously with N-fixation (both were measured by Raes et al 2020 although no relationship was reported; it has been implied that N-
350 fixation leads to an increase in the nitrate inventory; Mills et al., 2004), it likely has a role in redistributing newly fixed nitrogen, which is directly released as NH_4^+ or regenerated as NH_4^+ from the decomposition of released dissolved organic nitrogen (Glibert and Bronk, 1994; Mulholland et al., 2004; Newell et al., 2011). During this study, the seasonal low in dust deposition to the North Atlantic may have shifted resource constraints towards phosphate-Fe co-limitation, with implications for the extent and rate of N-fixation, and speculatively extending to the subsequent processes of N-
355 remineralisation.

A Primary Nitrite Maximum (PNM) was evident over the entire transect (Fig. 3e). A range of 0.05-0.50 µmol L^{-1} was measured, although sampling resolution may have limited the extent to which this feature was resolved (Beman, 2012; Meeder et al., 2012). Evidence suggests that nitrification has an important role in the formation and maintenance of the PNM against diffusive forces (Peng et al., 2018; Beman et al., 2012; Newell et al., 2013; Buchwald and Casciotti,
360 2013; Santoro et al., 2013; Meeder et al., 2012), with potential contributions from NO_2^- release by phytoplankton (Beman et al., 2012; Santoro et al 2013). This study is unable to inform the debate surrounding PNM formation as the isotope dilution approach adopted here does not discriminate between the processes contributing to NO_2^- regeneration (ammonium oxidation, algal NO_2^- release and potentially a photolytic route which produces NO_2^- from NO_3^- (Zafiriou and True, 1979) and humic substances (Kieber and Seaton, 1999)). The release of NO_2^- by phytoplankton is most
365 frequently associated with an intracellular resource imbalance linked to dynamic transitions (e.g. vertical mixing across a light gradient; Santoro et al., 2013; Lomas and Lipschultz, 2006; Meeder et al., 2012) which indicates that ammonium oxidation likely dominated the contribution to R_{NO2}. Across all depths, the oxidation of NH_4^+ lead to an average NO_2^- turnover of 38.5 days (range 0.4-335 days) within the North Atlantic Gyre compared to an average of 37 days (range 2.9-160 days) for the South Atlantic Gyre. For the PNM, a range of 3-40 days was reported within the California current
370 system (Santoro et al., 2013) and 33-178 days in the Arabian Sea (Buchwald and Casciotti, 2013).

The dissolved oxygen concentration was generally observed to be ~200-300 µmol L^{-1}, with variability linked to seawater temperature (Fig. 4d). Dissolved oxygen concentration has been shown to structure the activity and distribution of nitrifying organisms (Ward, 2002, Beman et al., 2008; 2012), especially within low oxygen environments (Beman et al., 2008; Bouskill et al., 2012). A low oxygen feature of the 0.1 % sPAR equatorial upwelling
375 water was distinguished in a series of correlation plots (Fig. 4 a-c), linked to relatively low temperature and salinity in combination with a very high NO_3^- concentration. This well documented oxygen minimum region is related to large scale circulation causing weak ventilation (Kartensen et al., 2008). This relative extreme in a combination of physico-

chemical conditions did not result in distinct elevations of R_{NO2} (Fig. 4d). Similar results were noted by Shoizaki et al., (2016) in the North Pacific Ocean, where dissolved oxygen concentrations approaching 50 µmol L^{-1} were not associated

380   with an enhanced rate of nitrification. Nitrification within low-oxygen environments is of interest as it links N-inputs to marine environments via N-fixation to N-losses via denitrification and anaerobic ammonium oxidation (annamox), processes which are characteristically associated with marine regions of extremely low oxygen concentration (Francis et al., 2007; Ward et al., 1989).

4.4 Biological context

385   Profiles of biological parameters (chlorophyll-a, pico-eukaryote and bacterial abundance) demonstrated apparent vertical structure. The chlorophyll-a distribution indicated that photosynthetic cells were present throughout the depth range used for R_{NO2} measurements. The presence of measurable chlorophyll-a implied the potential production and release of dissolved organic matter, in addition to organic matter released upon cell rupture (via grazing or viral attack). In contrast to the deep chlorophyll-a and picoplankton abundance maxima, bacterial cell profiles tended to describe

390   higher abundance towards the well-lit region of the water column. Assuming that bacterial cell abundance reflected resource availability, the observed distribution implied the availability of photosynthetically derived labile DOM throughout the photic zone (noting that the DCM represents only a small fraction of water column productivity and biomass; Marañon et al., 2000), and consequently the regeneration of NH_4^+. While the subsequent fate of regenerated NH_4^+ would relate to environmental factors that shape the open ocean ecosystem, molecular evidence supports the

395   potential for nitrifying activity throughout the surface ocean (Church et al., 2010; Santoro et al., 2010).

4.5 R_{NO2}, measurements within the study.

Ammonium oxidation was consistently measured at three sPAR depths within the physical, chemical and biological context described above (Fig. 6; Fig. 7a-c), indicating that NH_4^+ was available to support an oxidation rate of 0.02-13.27 nmol L^{-1} d^{-1}. When integrated between the surface and 0.1% sPAR, the range was 0.01-0.91 mmol m^{-2} d^{-1}. In their

400   study of the tropical eastern Pacific and Gulf of California, Beman et al., (2012) report a range of 1.38-7.72 mmol m^{-2} d^{-1} in the upper 300 m although only 1.5-42 % of integrated ammonium oxidation was associated with depths shallower than 1 % sPAR. Assuming a range of 10-100 nmol L^{-1} NH_4^+ at sampling depths throughout the transect, a range consistent with historical measurements (Clark et al., 2008; British Oceanographic Data Centre data archives; www. BODC.ac.uk), a specific rate of 0.011-0.113 d^{-1} was derived. This basin-scale range is comparable to that typically

405   applied in biogeochemical models, reported to be 0.02 to 0.1 d^{-1} (Moore et al., 2002; Wang et al., 2006; Christian et al., 2002; Jiang et al., 2003), although in their global model Yool et al. apply a value of 0.2 d^{-1} (Yool et al., 2007).

The vertical distribution and magnitude of R_{NO2} rates were consistent with previous observations, whereby low but detectable rates were measured within the well-lit ocean, a peak in ammonium oxidation rates was measured at 1 % sPAR, and a decline in rates was measured as depth increased below 1 % sPAR (Fig. 6; 7d, e; Al-Qutob et al., 2002;

410   Santoro et al., 2013; Shiozaki et al., 2016; Newell et al., 2013; Peng et al., 2018; Beman et al., 2012). The causes for this distribution are a continuing subject of debate, but ultimately reflect a balance between multiple factors including the provision of labile organic matter supporting the regeneration of NH_4^+, competition for this resource from other microbes including photosynthetic cells, and grazing pressure by mixotrophs and heterotrophic protists upon the nitrifying community.

415   A striking feature of the R_{NO2} data set was the 1 % sPAR rate range associated with south Atlantic stations (Fig. 7d), the mean of which was significantly greater than that measured in the North Atlantic Gyre. Indeed, by extrapolating vertically integrated values across a comparable distance into each hemisphere from the equator, we derive that the amount of NH_4^+-N oxidised to NO_2^- was 0.36 mol N d^{-1} over a 1 m x 4457 km distance north of the equator and 0.72 mol N d^{-1} over a 1 m x 4637 km distance south of the equator. We are unable to conclusively explain this novel

420   distinction between hemispheres. However, it is recognised that the Atlantic gyres have persistent biogeochemical differences in dust deposition, the inorganic nutrient regime and biological features such as N-fixation (Baker and Jickells, 2017; Moore et al., 2009; Ussher et al., 2013) that likely shape and influence broader biological activity within the surface ocean of each Atlantic gyre. Seasonality may be an additional component that contributes towards this hemispheric distinction. In their analysis of multiple AMT transects, Poulton et al. (2006) noted that high rates of

425   carbon fixation at the sub-surface chlorophyll-a maximum characterizing SATL stations during October were potentially linked to the onset of spring conditions. At this time, nutrients supplied by winter mixing to the sub-surface

chlorophyll-a maximum in combination with basin scale changes in irradiance, support the growth of larger eukaryotic phytoplankton (Letelier, 2004). The associated seasonal production of organic material would inevitably lead to an increase in decomposition and inorganic nutrient regeneration (including nitrification). Multivariate analysis, which

430   identified an association between ammonium oxidation and chlorophyll-a, light duration and nutrients, provided support for this association, as discussed below.

Multivariate approaches were used to investigate potential structure within the data and to examine relationships between ammonium oxidation and environmental variables. However, it is first worth considering limitations of the data set used for this analysis. While there is strong evidence to suggest that ammonium oxidation reflected ammonium

435   oxidation activity rather than alternative sources of NO_2^-, the measurement does not distinguish between archaeal or bacterial nitrifiers, which likely dominate separate niches within depth profiles (Benman et al., 2012). Nor does it consider the influence of changes in nitrifier community composition along the extended transect. Microbial cell abundance is no indication of the activity of specific microbial groups, or their importance to biological processes. Chlorophyll-a concentration does not reflect changes in species composition, or necessarily biomass, which are known

440   to change in response to environmental forcing within the Atlantic Ocean (Poulton et al 2006). Within these limitations, the PCA ordination of the entire data set (Fig. 9) demonstrated greater similarity within a sampling depth, equating to horizontal scales of hundreds of kilometres, than between sampling depths equating to vertical scales of tens of meters. A similar result was previously observed (Poulton et al., 2017), implying that distinct niches exist between depth horizons.

445   Statistical analysis aimed to identify the subset of explanatory variables that, in combination, best matched the observed pattern of ammonium oxidation rates. This match was provided by a combination of chlorophyll-a concentration, light duration and silicate concentration. A similar outcome was reported by Shiozaki et al., (2016) in their study of the oligotrophic North Pacific, in which a correlation between the activity of photosynthetic cells and ammonium oxidation was reported, although this relationship was not consistently observed at all sampling stations.

450   Chlorophyll-a and light duration as explanatory variables were common to all three sampling depths while depth-specific relationships incorporated additional variables. These results implied that, either directly or indirectly, ammonium oxidation responded to a product of actively photosynthesising cells (as opposed to other microbes identified by AFC). The production and release of labile dissolved organic matter during photosynthetic activity and its subsequent decomposition to regenerate NH_4^+ is an intuitive (and potentially spatially/temporally close) link between

455   photosynthetic cells and nitrifying organisms that could be supported by this insight. However, a role for silicate has not previously been reported, potentially highlighting a link to diatoms. Diatoms are relatively large, mineralising phytoplankton capable of rapid growth that contribute significantly to organic matter production and export in oligotrophic environments (Klass and Archer, 2006; Scharek et al., 1999). Alternatively, and perhaps more likely, silicate may be viewed as a tracer for sporadic nutrient inputs from below the nutricline (to include NO_3^-, PO_4^{3-}) that

460   stimulate short-term growth of photosynthetic cells in oligotrophic environments (Poulton et al., 2006). In contrast to other resources supplied by vertical mixing (e.g. NO_3^-, PO_4^{3-}), silicate is only utilised by diatoms which represent a fraction of the microbial community. It is reasonable to expect that following a localised mixing event, elevated silicate concentrations persist for longer than the simultaneously introduced NO_3^- and PO_4^{3-}, which are drawn down due to localised increases in primary productivity. Silicate effectively becomes a tracer for water that hosts the products of

465   active or recently enhanced productivity, with subsequent decomposition and nutrient regeneration.

The current view of low nutrient environments sees a dominant role for the picoplankton community which supports the microbial food web, with the sporadic growth of large phytoplankton following episodic nutrient inputs due to localised short-term physical instability (Carpenter et al., 1999; Scharek et al., 1999; Dandonneau et al., 2003; Poulton et al., 2006). Increased nutrient availability favours larger and faster growing cells that outcompete the picoplankton to

470   transiently dominate the microbial community in open ocean environments (Kiørbe, 1993). Organic matter released during such transient events (directly from living cells or following cell lysis) would support a short-term localised increase in N-regenerating activity, including ammonium oxidation. Evidence indicates that archaea, which frequently dominate the euphotic zone nitrifying community, possess a high resource affinity and respond rapidly to NH_4^+ pulses in culture (Martens-Habbena et al., 2009; Beman et al., 2012). Whether the statistically significant link between rates of

475   ammonium oxidation and a combination of chlorophyll-a, light duration and silicate relates to diatoms specifically (which have an absolute requirement for silicate and are obligate phototrophs i.e. they do not express mixotrophy unlike most other photosynthetic plankton, a nutritional mode that affords flexibility in resource limited environments and decreases dependence upon photosynthetic CO_2 fixation; Mitra et al., 2014) or more likely relates to a broader

480 stimulation of transient micro-plankton growth remains to be tested. Should nitrifying activity be responding to a chain of events in the very recent past, instantaneous rates of nitrification may not be fully explained by routine measurements of extant environmental conditions, such as those used in the present study. A detailed examination of labile DON production and decomposition may be required in combination with studies of nitrification.

Conspicuously prominent ammonium oxidation rates were associated with stations 28 °S and 39 °S, with measured ranges of 1.5-8.6 nmol L^{-1} d^{-1} and 1.3-13.3 nmol L^{-1} d^{-1} respectively (Fig. 4d; 7a-c). Selected biogeochemical
485 characteristics further distinguished station 39 °S (high P*, O$_2$ concentration, lower salinity and temperature; Fig. 3; 4) although those of station 28 °S were typical of the province. The use of Earth Observation data (sea surface temperature, ocean colour) revealed no anomalous features co-incident with these stations. However, Sea Surface Height Anomaly (SSHA) data evidenced that 28 °S and 39 °S were associated with mesoscale eddy features at the point of sampling (Fig. 9). Analysis revealed that no other stations of this study coincided with discernible mesoscale eddy
490 features at the point of sampling.

Eddy 39 °S was locally generated. In contrast, eddy 28 °S likely originated within the Agulhas Retroflection, traversing and potentially influencing SAG biogeochemistry before dissipating on the Brazilian shelf some 3.5 years later. Nencioli et al., (2018) tracked similar features, showing that they provided a coherent transport of water masses, preserving some of the physical and biological signals over more than two years. The vertical flux of inorganic nutrients
495 induced by the dynamics of traversing eddies has been argued to balance the Sargasso Sea nutrient budget (McGillicuddy et al., 1998). Similarly, the NO$_3^-$ deficit observed between new production requirements and diffusive NO$_3^-$ supplies in the Atlantic Gyres may be reconciled to some extent by eddy dynamics (Planas et al., 1999). While the nutrient regime of 28 °S was comparable to the provincial average, elevated ammonium oxidation (some 2-6 times higher than the provincial average) implied unusual biological activity; such activity is not sustained in isolation, but
500 must couple (over appropriate scales of space/time) to the activity of other biological processes (e.g. nutrient acquisition, photosynthetic growth, DON production and decomposition, NO$_2^-$ oxidation), presumably supported by new nutrients physically introduced into the photic zone by eddy dynamics. Unfortunately, given that only 3 ammonium oxidation rate observations were made at station 28 °S, located at the edge of a feature which measured approximately 300 km in diameter, little can be said about how representative of the feature this activity is, the relevance to broader
505 nitrogen cycling activity or its significance as a source of atmospheric N$_2$O (Dore and Karl, 1996).

4.6 Conclusions

This study reported relatively high-resolution measurements of ammonium oxidation rate at the oceanic basin scale. Ammonium oxidation took place at all locations investigated, adding to evidence that this process is widely distributed and active within the sunlit ocean. Considering all rate data, results implied that more active nitrogen cycling took place
510 in the South compared to the North Atlantic Gyre. While seasonality may contribute towards this hemispheric distinction, we speculate that this is a persistent feature. Historical AMT data sets demonstrate the broad inter-annual consistency of biogeochemical distributions and features to which ammonium oxidation rate significantly related. Should this testable hypothesis be substantiated, it would allude to a broader biogeochemical distinction between Atlantic gyres as the process of ammonium oxidation is intrinsically linked to other microbial processes that cycle
515 resources. By extension, as chemolithoautotrophs, nitrifiers fix CO$_2$ concurrently with nitrifying activity. Nitrifier mediated C-fixation in the South Atlantic Gyre would also exceed that of the North. A statistical analysis of observational data indicated that ~65% of variability in ammonium oxidation rate was explained through co-variability with environmental variables. A previously observed link to photosynthetic cells (Shiozaki et al., 2016) was supported here, and summarised as a significant relationship between ammonium oxidation rate and a combination of
520 chlorophyll-a concentration, light duration and silicate. We speculate that as an indication of recent physical instability, silicate transiently marks seawater that hosts the products of active or recently enhanced photosynthetic productivity, with subsequent organic matter decomposition and nutrient regeneration. This leads us to conclude that a role for DOM, and specifically the short-term production, release and decomposition of labile material is amongst the factors contributing to the unexplained variability in ammonium oxidation.

525 Two mesoscale eddies supported very high rates of ammonium oxidation, an observation previously unreported. Although the limited number of observations do not permit a meaningful analysis, results highlight the possibility that eddies which traverse the South Atlantic Gyre may disproportionately influence mixed layer biogeochemistry and ocean-atmosphere gas exchange.

Data availability

530   All AMT 19 metadata can be downloaded from the British Oceanographic Data Centre website: https://www.bodc.ac.uk/data/hosted_data_systems/amt/, in addition to ammonium oxidation rate data (doi:10.5285/56df6379-5b2b-160b-e053-6c86abc01f07) and flow cytometry data (10.5285/a2104adc-e994-6789-e053-6c86abc0d557).

Author contribution

535   DRC – designed experiments, undertook sample and data analysis, written manuscript; APR – conducted N-cycle fieldwork investigations, contributed to manuscript preparation; CF - conducted N-cycle fieldwork investigations; CH - conducted inorganic nutrient analysis of fieldwork samples; LA – mass spectrometry sample analysis; PJS - statistical analysis, contributed to manuscript preparation; GDQ - satellite data analysis, contributed to manuscript preparation; SG – satellite data analysis; GL –data analysis, contributed to manuscript preparation; GT- conducted flow cytometry
540   analysis of fieldwork samples, contributed to manuscript preparation.

Competing interests

The authors declare that they have no conflict of interest.

Acknowledgments

References

550   Al-Qutob, M., Hase, C., Tilzer, M. M., and Lazar, B.: Phytoplankton drives nitrite dynamics in the Gulf of Aqaba, Red Sea. Marine Ecology Progress Series. 239, 233-239, doi:10.3354/meps239233, 2002.

Azam, F., Fenchel, T., Field, G., Graf, J. S., Meyer-Reil, L. A., and Thingstad, F.: The ecological role of water-column microbes in the sea. Mar. Ecol. Prog. Ser. 10, 257–263. doi:10.3354/meps010257, 1983.

Baker, A. R., and Jickells, T. D.: Atmospheric deposition of soluble trace elements along the Atlantic Meridional
555   Transect (AMT). Prog. Oceanogr. 158, 41-51, doi:10.1016/j.pocean.2016.10.002, 2017.

Beman, J. M., Popp, B. N., and Francis, C. A.: Molecular and biogeochemical evidence for ammonia oxidation by marine Crenarchaeota in the Gulf of California. ISME J 2: 429–441, doi:10.1038/ismej.2007.118, 2008.

Beman, J., Chow, C-E., King, A., Feng, Y., Fuhrman, J. A., Andersson, A., Bates, N.R., Popp, B. N. and Hutchins, D.A.: Global declines in oceanic nitrification rates as a consequence of ocean acidification. Proc. Natl. Acad.
560   Sci. USA 108, 208–213, doi:10.1073/pnas.1011053108 2011, 2011.

Beman, J. M., B. N. Popp, S. E. and Alford. S. E.: Quantification of ammonia oxidation rates and ammonia-oxidizing archaea and bacteria at high resolution in the Gulf of California and eastern tropical North Pacific Ocean. Limnol. Oceanogr. 57, 711– 726. doi:10.4319/lo.2012.57.3.0711, 2012.

Bernhard, A. E., Landry, Z. C., Blevins, A., de la Torre, J. R., Giblin, A. E., and Stahl, D. A.: Abundance of ammonia-
565   oxidizing Archaea and Bacteria along an estuarine salinity gradient in relationship to potential nitrification rates, Appl. Environ. Microbiol. 76, 1285–1289, doi:10.1128/AEM.02018-09, 2010.

Blackburn, T. H.: Method for measuring rates of NH_4^+ turnover in anoxic marine sediments, using a $^{15}N-NH_4^+$ dilution technique. Appl. Environ. Microbiol. 37, 760–765, 1979.

Bouskill, N. J., Eveillard, D., Chien, D., Jayakumar, A., Ward, B. B.: Environmental factors determining ammonia-
570 oxidizing organism distribution and diversity in marine environments. Environ. Microbiol. 14, 714-29, doi:
10.1111/j.1462-2920.2011.02623.x, 2012.

Buesseler, K. O., and Boyd, P. W.: Shedding light on processes that control particle export and flux attenuation in the
twilight zone of the open ocean. Limnol. Oceanogr. 54, 1210–1232. doi:10.4319/lo.2009.54.4.12102009, 2009.

Buchwald, C., and Casciotti, K. L.: Isotopic ratios of nitrite as tracers of the sources and age of oceanic nitrite. Nat.
575 Geosci. 6, 308–13, doi:10.1038/ngeo1745, 2013.

Caperon, J., Schell, D., Hirota, J., and Laws, E.: Ammonium excretion rates in Kaneohe Bay, Hawaii, measured by a
^{15}N isotope dilution technique. Mar. Biol. 54, 33–40, 1979.

Carpenter, E. J., Montoya, J. P., Burns, J., Mulholland, M. R., Subramaniam, A., and Capone, D. G.: Extensive bloom
of a N_2-fixing diatom/cyanobacterial association in the tropical Atlantic Ocean. Mar. Ecol. Prog. Ser. 185, 273–
580 283, doi: 10.3354/meps185273, 1999.

Christian, J. R., Verschell, M. A., Murtugudde, R., Busalacchi, A. J., and McClain, C. R.: Biogeochemical modelling of
the tropical Pacific Ocean. I: Seasonal and interannual variability. Deep-Sea Research Part II 49, 509–543,
doi:10.1016/S0967-0645(01)00110-2, 2002.

Church, M. J., Karl, D. M., and DeLong, E. F.: Abundances of crenarchaeal amoA genes and transcripts in the Pacific
585 Ocean, Environ. Microbiol., 12, 679–688, 2010. doi:10.1111/j.1462-2920.2009.02108.x, 2010.

Clark, D. R., Flynn, K. J., Owens, N. J. P.: The large capacity for dark nitrate-assimilation in diatoms may overcome
nitrate limitation of growth. New Phytol. 155, 101-108, doi:10.1046/j.1469-8137.2002.00435.x, 2002.

Clark, D. R., Fileman, T. W., and Joint, I.: Determination of ammonium regeneration rates in the oligotrophic ocean by
gas chromatography/mass spectrometry. Mar. Chem. 98, 21–130, doi:10.1016/j.marchem.2005.08.006, 2006.

590 Clark, D. R., Rees, A. P., and Joint, I.: A method for the determination of nitrification rates in oligotrophic marine
seawater by gas chromatography/mass spectrometry. Mar. Chem. 103, 84–96, doi:
10.1016/j.marchem.2006.06.005, 2007.

Clark, D. R., Rees, A. P., and Joint, I.: Ammonium regeneration and nitrification rates in the oligotrophic Atlantic
Ocean: Implications for new production estimates. Limnol. Oceanogr. 53, 52–62, doi:10.2307/40006149, 2008.

595 Clark, D. R., Brown, I. J., Rees, A. P, Somerfield, P. J., and Miller, P. I.: The influence of ocean acidification on
nitrogen regeneration and nitrous oxide production in the northwest European shelf sea. Biogeosciences 11,
4985–5005, doi:10.5194/bgd-11-3113-2014, 2014.

Clarke, K. R., and Warwick, R. M.: Quantifying structural redundancy in ecological communities. Oecologia 113, 278-
289, doi:10.1007/s004420050379, 1998.

600 Clarke, K. R., Somerfield, P. J., and Gorley, R. N.: Testing of null hypotheses in exploratory community analyses:
similarity profiles and biota-environment linkage. J. Exp. Mar. Biol. Ecol. 366, 56-69, doi:
10.1016/j.jembe.2008.07.009, 2008.

Clarke, K. R., Gorley, R. N., Somerfield, P. J., and Warwick, R. M.: Change in marine communities: an approach to
statistical analysis and interpretation, 3rd edn. PRIMER-E, Plymouth. 256 pp, 2014.

605 Dandonneau, Y., Vega, A., Loisel, H., du Penhoat, Y., and Menkes, C.: Oceanic Rossby waves acting as a hay rake for
ecosystem floating by-products. Science 302, 1548–1551, doi:10.1126/science.1090729, 2003.

Dore, J. E., and Karl, D. M.: Nitrification in the euphotic zone as a source for nitrite, nitrate and nitrous oxide at Station
ALOHA. Limnol. Oceanogr. 41, 1619-1628, doi:10.4319/lo.1996.41.8.1619, 1996.

610 Emerson, S., Mecking, S., and Abell, J.: The biological pump in the subtropical North Pacific Ocean: Nutrient sources, Redfield ratios, and recent changes. Global Biogeochem. Cy. 15, 535-554, doi:10.1029/2000GB001320, 2001.

Eppley, R.W., and Peterson, B. J.: Particulate organic matter flux and planktonic new production in the deep ocean. Nature 282, 677-680, 1979.

Fawcett, S. E., Ward, B. B., Lomas, M. W., and Sigman, D. M.: Vertical decoupling of nitrate assimilation and nitrification in the Sargasso Sea. Deep-Sea Research I 103, 64-72, doi:10.1016/j.dsr.2015.05.004, 2015.

615 Francis, C. A., O'Mullan, G. D., and Ward, B. B.: Diversity of ammonia monooxygenase (amoA) genes across environmental gradients in Chesapeake Bay sediments. Gobiology 1:129-140, doi:10.1046/j.1472-4669.2003.00010.x, 2003.

Francis, C., A., Beman, J. M., and Kuypers, M. M. M.: New processes and players in the nitrogen cycle: The microbial ecology of anaerobic and archaeal ammonia oxidation. ISMEJ. 1, 19–27, doi:10.1038/ismej.2007.8, 2007.

620 Giovanoni, S. J., and Vergin, K. L.: Seasonality in ocean microbial communities. Science, 335, 671-676, doi: 10.1126/science.1198078, 2012.

Glibert, P. M., and Bronk, D. A.: Release of dissolved organic nitrogen by marine diazotrophic cyanobacteria, Trichodesmium spp., Appl. Environm. Microbiol., 60, 3996–4000, doi:10.1128/AEM.60.11.3996-4000.1994, 1994.

625 Gruber, N., and Sarmiento, J. L.: Global patterns of marine nitrogen fixation and denitrification. Global Biogeochemical Cycles, 11, 235–266, doi:10.1029/97GB00077, 1997.

Horak, R. E. A., Qin, W., Schauer, A. J., Armbrust, E. V., Ingalls, A. E., Moffett, J. W., Stahl, D. A., and Devol, A. H.: Ammonia oxidation kinetics and temperature sensitivity of a natural marine community dominated by Archaea. ISME. 7, 2023-2033, doi:10.1038/ismej.2013.75, 2013.

630 IOC: Intergovernmental Oceanographic Commission, Paris. Protocols for the Joint Global Flux Study (JGOFS) core measurements. Manuals Guides 29. 1994.

Jiang, M. S., Chai, F., Dugdale, R. C., Wilkerson, F. P., Peng, T. H., and Barber, R. T.: A nitrate and silicate budget in the equatorial Pacific Ocean: a coupled physical-biological model study. Deep-Sea Research Part II 50:2971–2996, doi:10.1016/j.dsr2.2003.07.006, 2003.

635 Karstensen, J., Stramma, L., and Visbeck, M.: Oxygen minimum zones in the eastern tropical Atlantic and Pacific oceans. Prog. Oceanogr. 77, 331–350, doi:10.1016/j.pocean.2007.05.009, 2008.

Kieber, R. J., Li, A., and Seaton, P. J.: Production of nitrite from the photodegradation of dissolved organic matter in natural waters. Environmental Science and Technology, 33, 993–998, doi:10.1021/es980188a, 1999.

Kiørboe, T.: Turbulence, phytoplankton cell size, and the structure of pelagic food webs. Advances in Marine Biology
640 29, 2–72, doi:10.1016/S0065-2881(08)60129-7, 1993.

Klass, C., and Archer, D.: Association of sinking organic matter with various types of mineral ballast in the deep sea: Implications for the rain ratio. Global Biogeochemical Cycles 16, 1116, doi:10.1029/2001GB001765, 2002.

Letelier, R. M., Karl, D. M., Abbott, M. R., and Bidigare, R. R.: Light driven seasonal patterns of chlorophyll and nitrate in the lower euphotic zone of the North Pacific Subtropical Gyre. Limnology and Oceanography, 49,
645 508–519, doi:10.4319/lo.2004.49.2.0508, 2004.

Lomas, M. W., and Lipschultz, F.: Forming the primary nitrite maximum: Nitrifiers or phytoplankton? Limnology and Oceanography, 51, 2453-2467, doi: 10.4319/lo.2006.51.5.2453, 2006.

15

Lomas, M. W., Lipschultz, F., Nelson, D. M., Krause, J. W., and Bates, N. R.: Biogeochemical responses to late-winter
storms in the Sargasso Sea, I—Pulses of primary and new production. Deep-Sea Research I 56, 843–860,
650   doi:10.1016/j.dsr.2009.01.002, 2009.

Longhurst, A.: Ecological geography of the sea. Academic Press, 1998.

Maranñón, E., Holligan, P. M., Varela, M., Mourinõ, B., Bale, A.J.: Basinscale variability of phytoplankton biomass,
production and growth in the Atlantic Ocean. Deep Sea Research I 47, 825–857, doi: 10.1016/S0967-
0637(99)00087-4, 2000.

655   Martens-Habbena, W., Berube, P. M., Urakawa, H., de la Torre, J. R., and Stahl, D. A.: Ammonia oxidation kinetics
determine niche separation of nitrifying Archaea and Bacteria. Nature volume 461, 976–979,
doi:10.1038/nature08465, 2009.

McClain, C. R., Signorini, S. R., and Christian, J. R.: Subtropical gyre variability observed by ocean-color satellites.
Deep Sea Research Part II: Topical Studies in Oceanography 51, 281–301, doi:10.1016/j.dsr2.2003.08.002,
660   2004.

McGillicuddy, D. J., Jr, Robinson, A. R., Siegel, D. A., Jannasch, H. W., Johnson, R., Dickey, T. D., McNeil, J.,
Michaels, A. F., and Knap, A. H.: Influence of mesoscale eddies on new production in the Sargasso Sea, Nature,
394, 263–266, doi:10.1038/28367, 1998.

Meeder, E., Mackey, K. R. M., Paytan, A., Shaked, Y., Iluz, D., Stambler, N., Rivlin, T., Post, A. F., and Lazar, B.:
665   Nitrite dynamics in the open ocean—clues from seasonal and diurnal variations. Mar. Ecol. Prog. Ser. 453, 11-
26, doi:10.3354/meps09525, 2012.

Mills, M. M., Ridame, C., Davey, M., La Roche, J., and Geider, R. J.: Iron and phosphorus co-limit nitrogen fixation in
the eastern tropical North Atlantic. Nature volume 429:292–294, doi:10.1038/nature03632, 2004.

Mitra, A., Flynn, K. J., Burkholder, J. M., Berge, T., Calbet, A., Raven, J. A., Graneli, E., Glibert, P. M., Hansen, P. J.,
670   Stoecker, D. K., Thingstad, F., Tillmann, U., Våge, S., Zubkov, M.: The role of mixotrophic protists in the
biological carbon pump. Biogeosciences 11, 995–1005, doi:10.5194/bg-11-995-2014, 2014.

Moore, C. M., Mills, M. M., Achterberg, E. P., Geider, R. J., LaRoche, J., Lucas, M. I., McDonagh, E. L., Pan, X.,
Poulton, A. J., Rijkenberg, M. J. A., Suggett, D. J., Ussher, S. J., and Woodward, E. M. S.: Large-scale
distribution of Atlantic nitrogen fixation controlled by iron availability. Nature Geoscience 2, 867-871,
675   doi:10.1038/NGEO667, 2009.

Moore, C. M., Mills, M.M., Arrigo, K. R., Berman-Frank, I., Bopp, L., Boyd, P. W., Galbraith, E. D., Geider, R. J.,
Guieu, C., Jaccard, S. L., Jickells, T. D., La Roche, J., Lenton, T. M., Mahowald, N. M., Marañón, E., Marinov,
I., Moore, J. K., Nakatsuka, T., Oschlies, A., Saito, M. A., Thingstad, T. F., Tsudaand, A., and Ulloa, O.:
Processes and patterns of oceanic nutrient limitation. Nat. Geosci. 6, 701-710, doi:10.1038/NGEO1765, 2013.

680   Moore, J. K., Doney, S. C., Kleypas, J. A., Glover, D. M., and Fung I. Y.: An intermediate complexity marine
ecosystem model for the global domain. Deep-Sea Research Part II 49, 403–462, doi:10.1016/S0967-
0645(01)00108-4, 2002.

Mulholland, M. R., Bronk, D. A., and Capone, D. G.: Dinitrogen fixation and release of ammonium and dissolved
organic nitrogen by *Trichodesmium* IMS101, Aquatic Microb. Ecol., 37, 85–94, doi:10.3354/ame037085, 2004.

685   Mulholland, M. R.: The fate of nitrogen fixed by diazotrophs in the ocean. Biogeosciences. 4, 37-51, doi:10.5194/bg-4-
37-2007, 2007.

Nencioli, F., Dall'Olmo, G.,and Quartly, G. D.: Agulhas ring transport efficiency from combined satellite altimetry and
Argo profiles. Journal of Geophysical Research: Oceans, 123. doi:10.1029/2018JC013909, 2018.

Biogeosciences
Discussions

Open Access

EGU

Newell, S. E., Babbin, A. R., Jayakumar, A., and Ward, B. B.: Ammonia oxidation rates and nitrification in the Arabian
690   Sea. Global Biogeochem. Cyc. 25(4):GB4016, doi:10.1029/2010GB003940, 2011.

Newell, S. E., Fawcett, S. E., and Ward, B. B.: Depth distribution of ammonia oxidation rates and ammonia-oxidizer
       community composition in the Sargasso Sea. Limnol Oceanogr. 58, 491–1500, doi:10.4319/lo.2013.58.4.1491,
       2013.

Olson, R. J.: Differential photoinhibition of marine nitrifying bacteria: A possible mechanism for the formation of the
695   primary nitrite maximum. J. Mar. Res. 39, 227–238, doi:10.4319/lo.2006.51.5.2453, 1981.

Oschlies, A., and Garçon, V.: Eddy-induced enhancement of primary production in a model of the North Atlantic
       Ocean, Nature, 394, 266–269, doi: 10.1038/28373, 1998.

Palinska, K.A., Laloui, W., Bédu, S., Goer, S.L., Castets, A.M., Rippka, R., de Marsac, N.T.: The signal transducer P-II
       and bicarbonate acquisition in Prochlorococcus marinus PCC 9511, a marine cyanobacterium naturally deficient
700   in nitrate and nitrite assimilation. Microbiology 148, 2405–2412, doi:10.1099/00221287-148-8-2405, 2002.

Partensky, F., Hess, W. R., and Vaulot, D.: Prochlorococcus, a Marine Photosynthetic Prokaryote of Global
       Significance. Microbiol Mol Biol 63, 06–127, doi:10.1016/j.procbio.2007.09.010, 1999.

Peng, X., Fawcett, S. E., van Oostende, N., Wolf, M. J., Marconi, D., Sigman, D. M., and Ward, B. B.: Nitrogen uptake
       and nitrification in the subarctic North Atlantic Ocean. Limnol. Oceanogr. 63, 1462-1487,
705   doi:10.1002/lno.10784, 2018.

Planas. D., Agusti, S., Duarte, C. M., Granata, T. C., and Merino, M.: Nitrate uptake and diffusive nitrate supply in the
       Central Atlantic. Limnol. Oceanogr., 44, 116-126, doi:10.4319/lo.1999.44.1.011, 1999.

Polovina, J. J., Howell, E. A., and Abecassis, M.: Ocean's least productive waters are expanding, Geophys. Res. Lett.,
       35, L03618, doi:10.1029/2007GL031745, 2008.

710   Poulton, A. J., Holligan, P. M., Hickman, A., Kim, Y-N., Adey, T. R., Stinchcombe, M. C., Holeton, C., Root, S., and
       Woodward, E. M. S.: Phytoplankton carbon fixation, chlorophyll-biomass and diagnostic pigments in the
       Atlantic Ocean. Deep-Sea Res. II 53, 1593–1610, doi:10.1016/j.dsr2.2006.05.007, 2006.

Poulton, A. J., Holligan, P. M., Charalampopoulou, A., and Adey, T. R.: Coccolithophore ecology in the tropical and
       subtropical Atlantic Ocean: new perspectives from the Atlantic meridional transect (AMT) programme. Prog.
715   Oceanogr. 158, 150–170, doi:10.1016/j.pocean.2017.01.003, 2017.

Rafter, P. A., DiFiore, P. J., and Sigman, D. M.: Coupled nitrate nitrogen and oxygen isotopes and organic matter
       remineralization in the Southern and Pacific Oceans. J. Geophys. Res. 118, 4781-4794, doi:10.1002/jgrc.20316,
       2013.

Raes, E. J., van de Kamp, J., Bodrossy, L., Fong, A. A., Riekenberg, J., Holmes, B. H., Erler, D. V., Eyre, B. D., Weil,
720   S-S., and Waite, A. M.: N_2 Fixation and New Insights Into Nitrification From the Ice-Edge to the Equator in the
       South Pacific Ocean. Front. Mar. Sci. 7:389. doi:10.3389/fmars.2020.00389, 2020.

Rees, A. P., Nightingale, P. D., Poulton, A. J., Smyth, T., Tarran, G. A., and Tilstone, G. H.: The Atlantic Meridional
       Transect programme (1995-2016). Prog. Oceanogr. 158, 3-18, doi:10.1016/j.pocean.2017.05.004, 2017.

Santoro, A. E., Casciotti, K. L., and Francis, C. A.: Activity, abundance and diversity of nitrifying archaea and bacteria
725   in the central California Current, Environ. Microbiol., 12, 1989–2006, doi:10.1111/j.1462-2920.2010.02205.x,
       2010.

Santoro, A. E., Buchwald, C., McIlvin, M. R., and Casciotti, K. L.: Isotopic Signature of N_2O Produced by Marine
       Ammonia-Oxidizing Archaea. Science 333, 1282-1285, doi:10.1126/science.1208239, 2011.

Biogeosciences

Discussions

Open Access

EGU

730   Santoro, A. E., Sakamoto, C. M., Smith, J. M. Plant, J. N., Gehman, A. L., Worden, A. Z., Johnson, K. S., Francis, C. A., and Casciotti, K. L.: Measurements of nitrite production in and around the primary nitrite maximum in the central California current. Biogeosciences. 10, 7395-7410, doi:10.5194/bgd-10-5803-2013, 2013.

Sarmiento, J. L., Gruber, N., Brzezinski, M. A. and Dunne, J. P.: High-latitude controls of thermocline nutrients and low latitude biological productivity. Nature 427, 5660, doi:10.1038/nature10605, 2004.

Scharek, R., Tupas, L. M., and Karl, D. M.: Diatom fluxes to the deep sea in the oligotrophic North Pacific gyre at
735   Station ALOHA. Marine Ecology Progress Series 182, 55–67, doi:10.3354/meps182055, 1999.

Shiozaki, T., Ijichi, M., Isobe, K., Hashihama, F., Nakamura, K., Ehama, M., Hayashizaki, K., Takahashi, K., Hamasaki, K., and Furuya, K.: Nitrification and its influence on biogeochemical cycles from the equatorial Pacific to the Arctic Ocean ISME J. 10, 2184-97, doi :10.1038/ismej.2016.18, 2016.

Smith, J. M., Chavez, F. P., and Francis, C. A.: Ammonium Uptake by Phytoplankton Regulates Nitrification in the
740   Sunlit Ocean. PLoS ONE 9:e108173, doi:10.1371/journal.pone.0108173, 2014.

Smith, J. M., Damashek, J., Chavez, F. P., and Francis, C. A.: Factors influencing nitrification rates and the abundance and transcriptional activity of ammonia-oxidizing microorganisms in the dark northeast Pacific Ocean. Limnol. Oceanogr. 61, 596-609, doi:10.1002/lno.10235, 2016.

Somerfield, P. J., and Clarke, K. R.: Inverse analysis in non-parametric multivariate analyses: distinguishing groups of
745   associated species which covary coherently across samples. J. Exp. Mar. Biol. Ecol. 449, 261–273, doi:10.1016/j.jembe.2013.10.002, 2013.

Somerfield, P. J., Clarke, K. R., and Gorley, R. N.: Analysis of Similarities (ANOSIM) for 2-way layouts using a generalised ANOSIM statistic, with comparative notes on Permutational Multivariate Analysis of Variance (PERMANOVA). Austral Ecology, doi:10.1111/aec.13059, 2021.

750   Taylor, A. H., Harris, J. R. W., and Aiken, J.: The interaction of physical and biological processes in a model of the vertical distribution of phytoplankton under stratification. In: Nihoul, J.C.J. (Ed.), Marine Interfaces Echohydrodynamics. Elsevier Science, Amsterdam, The Netherlands, pp. 313–330, doi:10.1016/S0422-9894(08)71052-3, 1986.

Tuerena, R. E., Ganeshram, R .S., Geibert, W., Fallick, A. E., Dougans, J., Tait, A., Henley, S. F., and Woodward, E.
755   M. S.: Nutrient cycling in the Atlantic basin: The evolution of nitrate isotope signatures in water masses. Global Biogeochem. Cycles 29, 1830–1844, doi:10.1002/2015GB005164, 2015.

Tuerena, R. E., Williams, R. G., Mahaffey, C., Vic, C., Green, J. A. M., Naveira-Garabato, A., Forryan, A., and Sharples, J.: Internal Tides Drive Nutrient Fluxes Into the Deep Chlorophyll Maximum Over Mid-ocean Ridges. Global Biogeochem. Cyc. 33, 995-1009, doi:10.1029/2019GB006214, 2019.

760   Vet, W. W. J. M. de; Loosdrecht, M. C. M. van, and Rietveld, L. C.: Phosphorus limitation in nitrifying groundwater filters. Water Research. 46:1061-1069. doi: 10.1016/j.watres.2011.11.075, 2012.

Ussher, S. J., Achterberg, E. P., Powell, C., Baker, A. R., Jickells, T. D., Torres, R., and Worsfold, P. J.: Impact of atmospheric deposition on the contrasting iron biogeochemistry of the North and South Atlantic Ocean. Global Biogeochem. Cycl. 27, 1096–1107, doi:10.1038/s41467-018-03363-0, 2013.

765   Wang, X. J., Christian, J. R., Murtugudde, R., and Busalacchi, A. J.: Spatial and temporal variability in new production in the equatorial Pacific during 1980-2003: Physical and biogeochemical controls. Deep-Sea Research Part II 53, 677–697, doi:10.1016/j.dsr2.2006.01.023, 2006.

Ward, B. B.: Light and substrate concentration relationships with marine ammonium assimilation and oxidation rates. Mar. Chem. 16, 301–316. doi:10.1016/0304-4203(85)90052-0, 1985.

770   Ward, B. B., Glover, H. E., and Lipshultz, F.: Chemoauto-trophic activity and nitrification in the oxygen minimum zone
            off Peru. Deep-Sea Res. A 36: 1031–1051, doi:10.1016/0198-0149(89)90076-9, 1989.

      Ward, B. B.: Nitrification in aquatic systems. In: Capone DA (ed). Encyclopaedia of Environmental Microbiology.
            Wiley: New York, NY, USA, pp 2144–2167, doi:10.1002/0471263397.env287, 2002.

      Zafiriou, O. C., and True, M. B. : Nitrate photolysis in seawater by sunlight. Marine Chemistry, 8, 33–42,
775   doi:10.1016/0304-4203(79)90029-X, 1979.

      Zamora, L. M., and Oschlies, A.: Surface nitrification: A major uncertainty in marine N_2O emissions. Geophys. Res.
            Lett. 41(12):4247-4253, doi:10.1002/2014GL060556, 2014.

      Woodward, E. M. S., and Rees, A. P.: Nutrient distributions in an anticyclonic eddy in the North 490 East Atlantic
            Ocean, with reference to nanomolar ammonium concentrations. Deep-Sea Res. 491 48(4-5):775–794, doi:
780   10.1016/S0967-0645(00)00097-7, 2001.

      Yool, A., Martin, A. P., Fernández, C., and Clark, D. R.: The significance of nitrification for oceanic new production.
            Nature 447:999–1002, doi: 10.1038/nature05885, 2007.

785

Biogeosciences
Discussions

Open Access

EGU
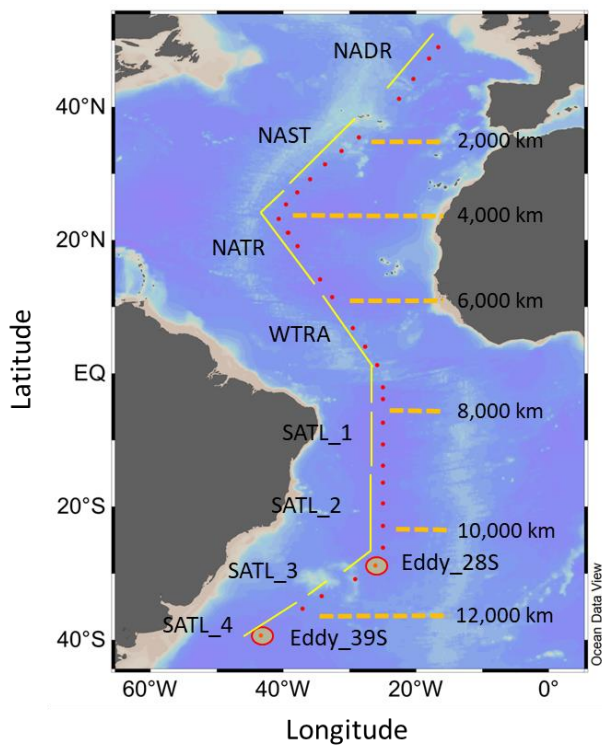
Figure 1. Map of the study area, indicating the position of sampling stations for N-cycle studies (red dots), the
approximate transect distance and the associated Longhurst provinces (Longhurst, 1998); North Atlantic Drift (NADR),
North Atlantic subtropical gyre (NAST), North Atlantic tropical gyre (NATR), Western tropical Atlantic (WTRA),
South Atlantic gyre (SATL). The location of two eddy features is also indicated.
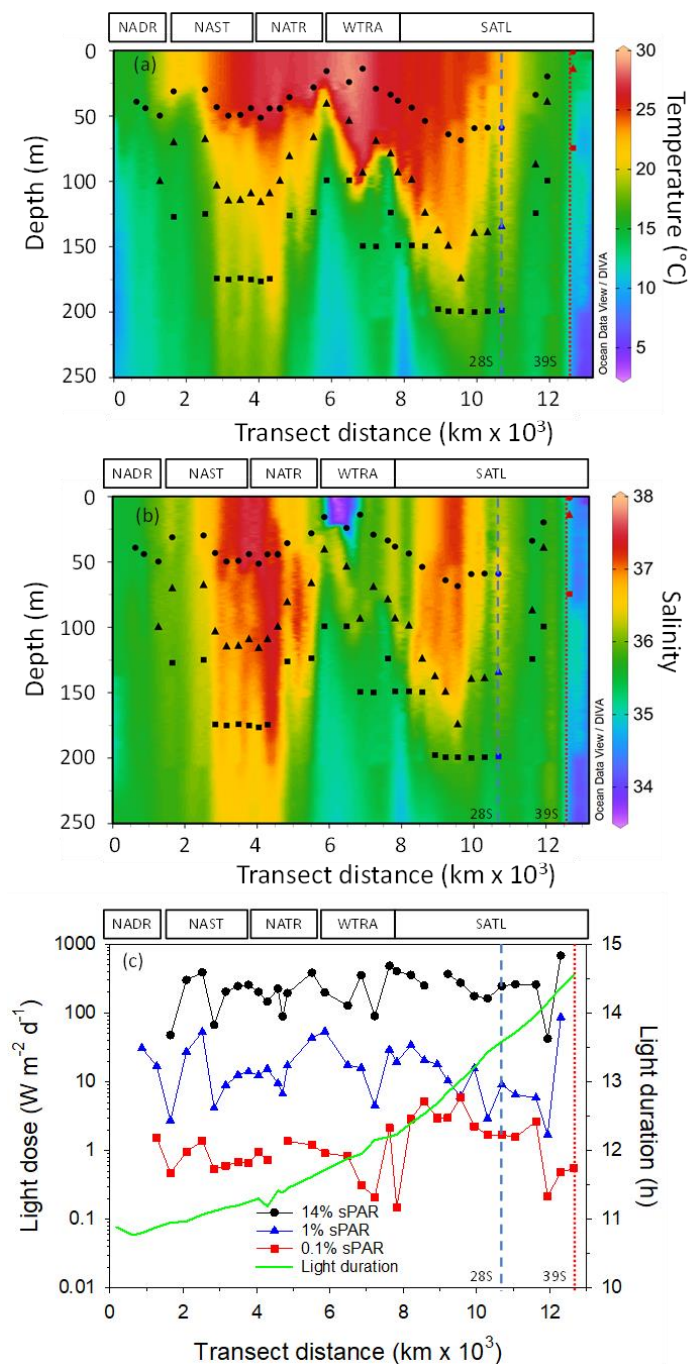
Figure 2. Contour plots of water column temperature (a) and salinity (b) measured during CTD rosette casts. The calculated daily light dose (PAR intensity x light phase duration) received at sampling depths is presented (c), in addition to the duration of the light phase (in hours). The approximate position of Longhurst provinces (defined in Fig. 1) is indicated. Symbols represent 14% sPAR (circle), 1% sPAR (triangle), 0.1% sPAR (square). The location of two eddy features is indicated by vertical dashed (28 °S) and dotted (39 °S) lines.

795

800
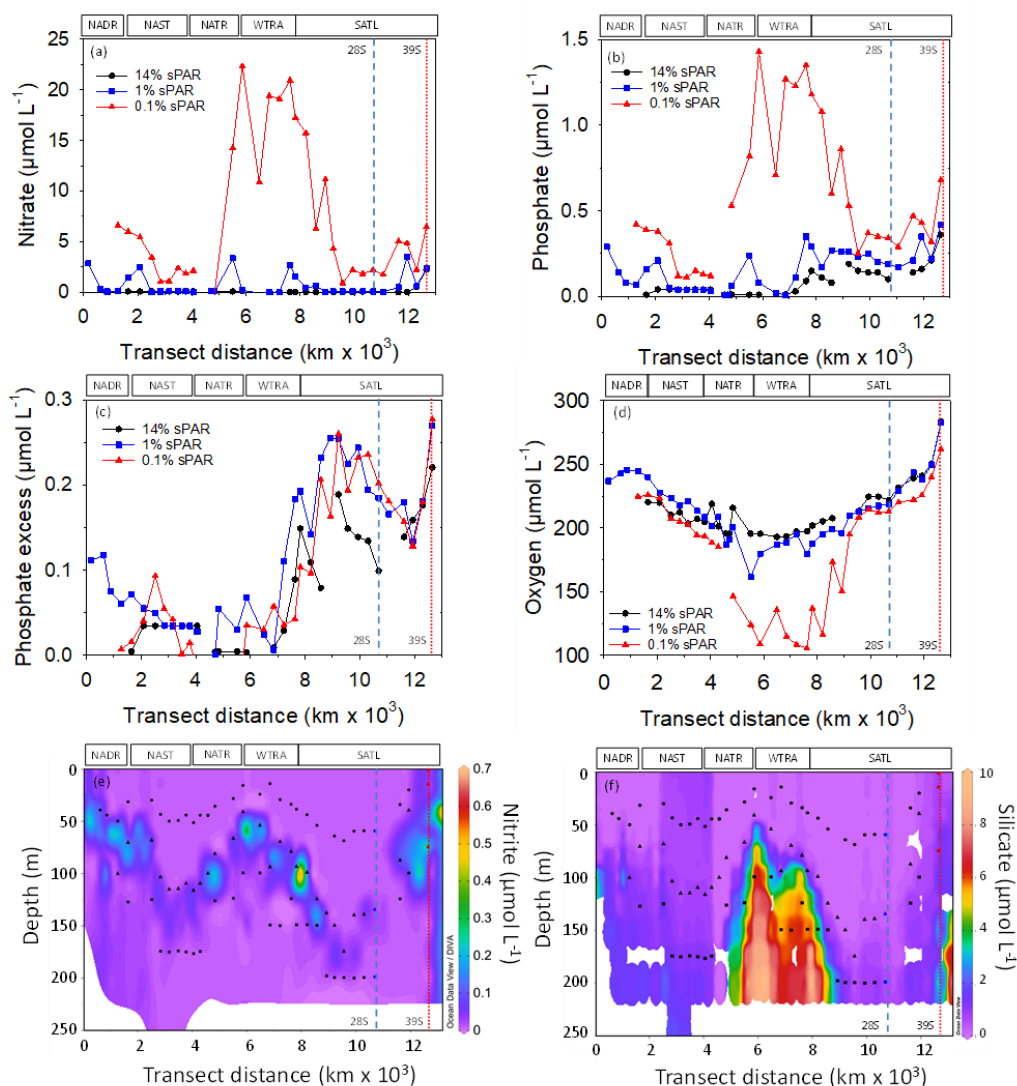
Figure 3. The concentration of nitrate (a), phosphate (b), phosphate excess (P*; c), oxygen (d), nitrite (e) and silicate (f). The location of two eddy features is indicated by vertical dashed (28 °S) and dotted (39 °S) lines. The approximate location of Longhurst provinces (defined in Fig. 1) is indicated. Symbols represent 14% sPAR (circle), 1% sPAR (triangle), 0.1% sPAR (square). The location of two eddy features is indicated by vertical dashed (28 °S) and dotted (39 °S) lines.
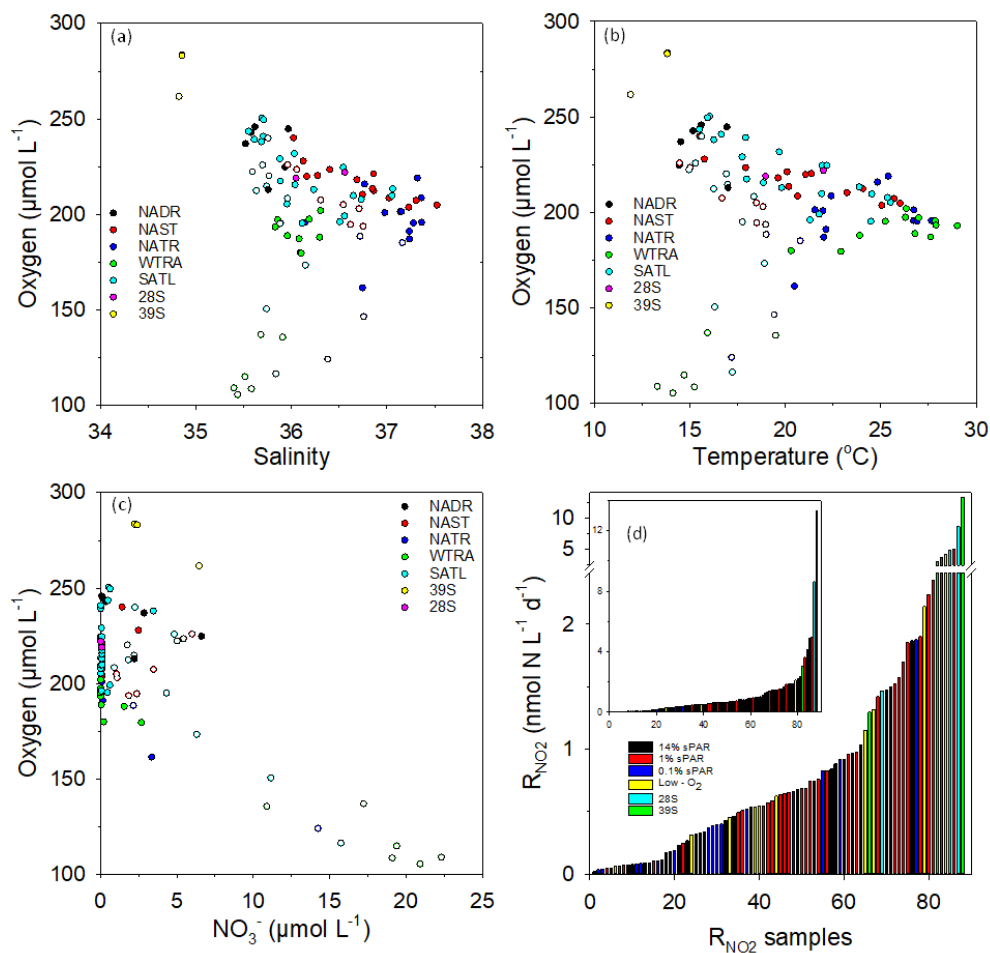
Figure 4. Plots of dissolved oxygen concentration vs salinity (a), temperature (b) and NO_3^- (c) within Longhurst provinces (defined in Fig. 1). Open circles represent 0.1% sPAR data, highlighting distinct characteristics associated with specific NATR/WTRA/SATL sampling points. To represent the distribution of rate data, the 88 R_{NO2} measurements were arranged in ascending order (d, insert has linear scale) with an indication of sampling depth, or the association with a specific feature (low oxygen, defined as < 150 µmol L^{-1}, or mesoscale eddy). Measurements within eddy features tend towards the high end of the scale, as do measurements at 1% sPAR. Low oxygen measurements show no clear distributional trend while 14% and 0.1% sPAR values tend towards the low end of the scale.

23
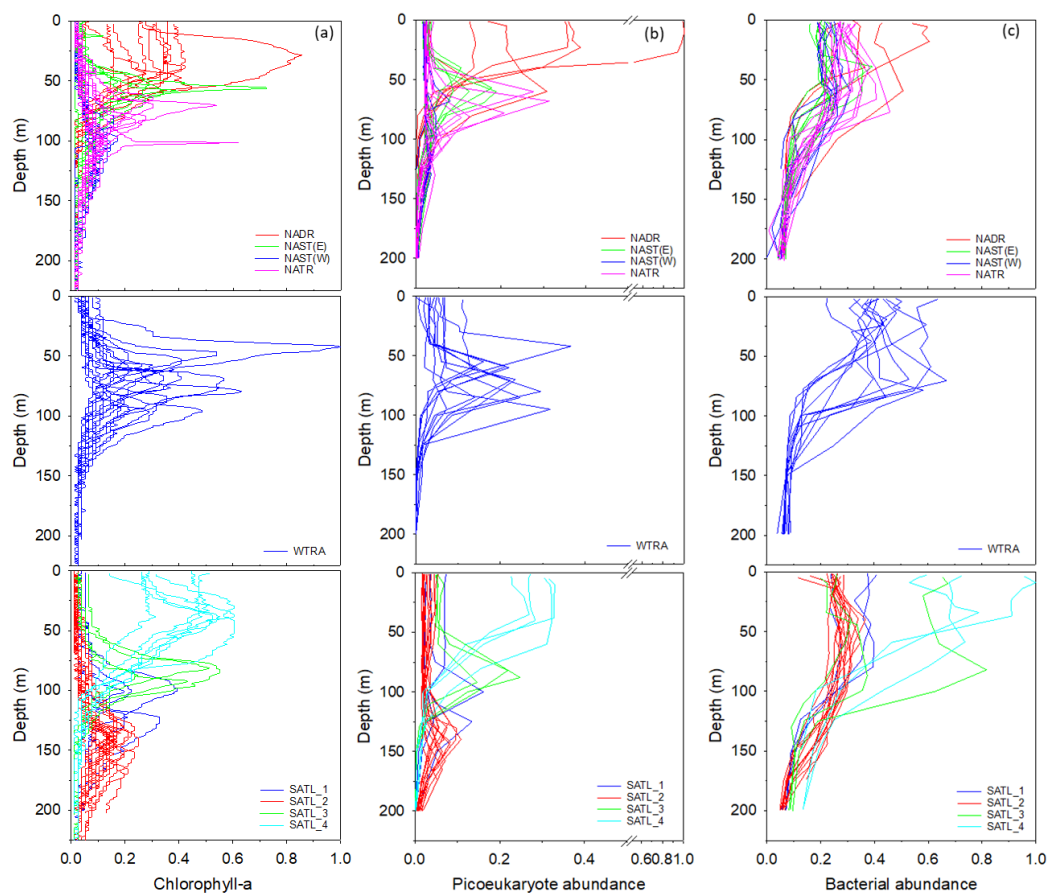
Figure 5. Profiles of chlorophyll-a concentration (a), the abundance of pico-eukaryotes (b) and bacteria (c) within Longhurst provinces (defined in Fig. 1). Data are presented as a ratio of the maximum value measured for each parameter throughout the transect. Profiles frequently describe comparable distributions within a defined province. However, data is sub-divided within the SATL province to illustrate apparent distinctions in vertical structure.
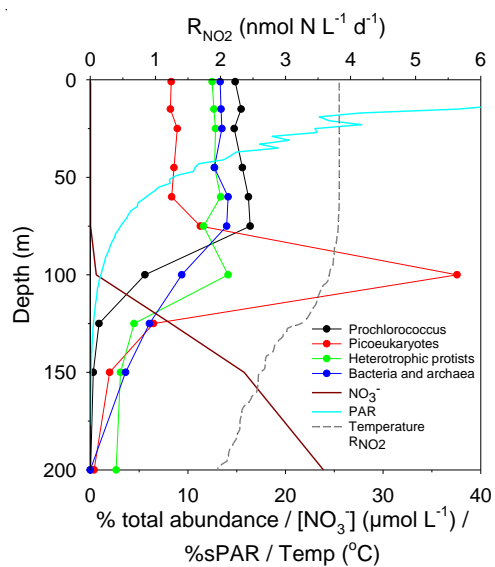
825

Figure 6. R_{NO2} measurements at 7 ^{0}S within the context of selected physical, chemical and biological measurements, illustrating relationships between water column characteristics.
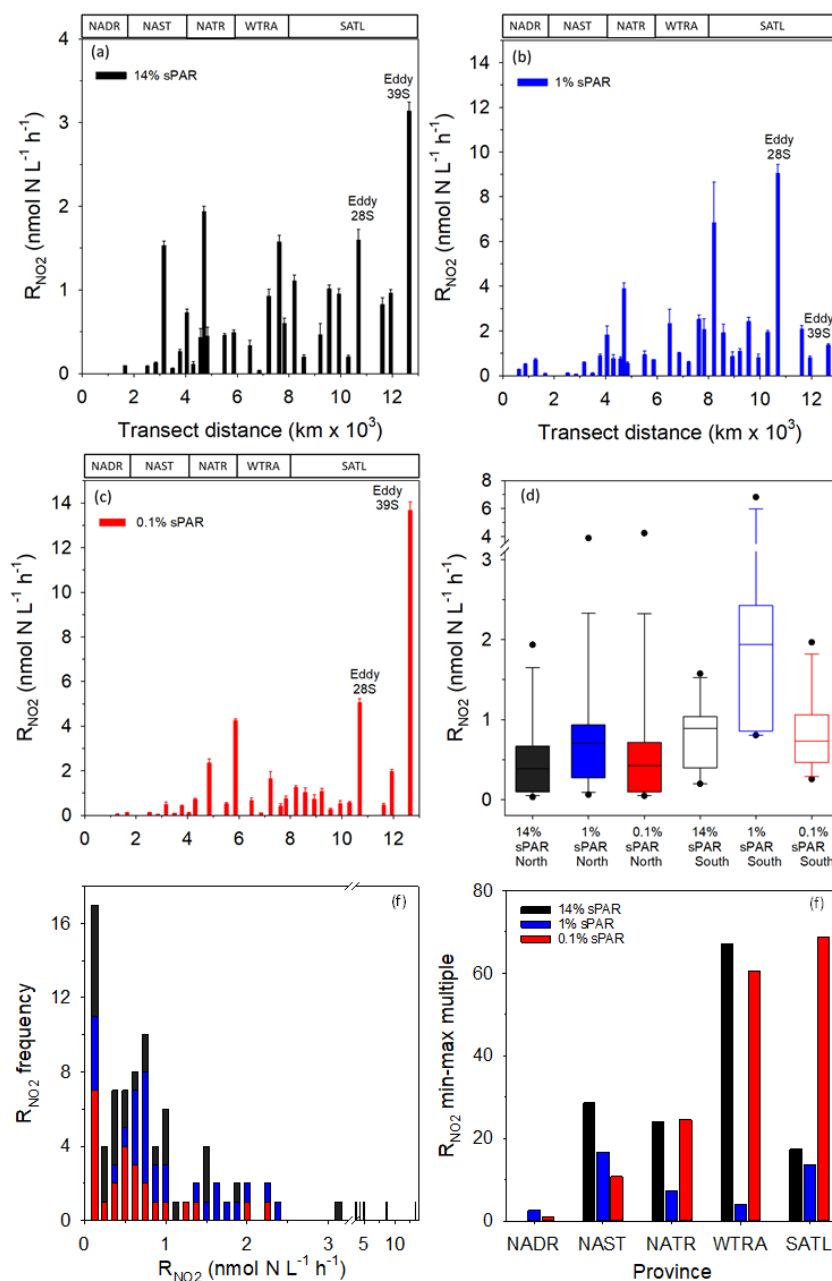
Figure 7. Volumetric rates of NO_2^- regeneration at 14% (a), 1% (b) and 0.1% (c) sPAR. Error bars represent two standard deviations of triplicate measurements. The approximate position of Longhurst provinces (defined in Fig. 1) is identified in these plots. The box plot (d) presents data for each hemisphere (excluding 28°S/39°S), as sPAR depths. The 10th, 25th, 75th and 90th data percentiles are presented with data median (line within box). A histogram of the rate distribution and frequency is presented in panel (e). An indication of R_{NO2} variability is presented in panel (f), as the number of minimum value multiples that equate to the largest value within each province.
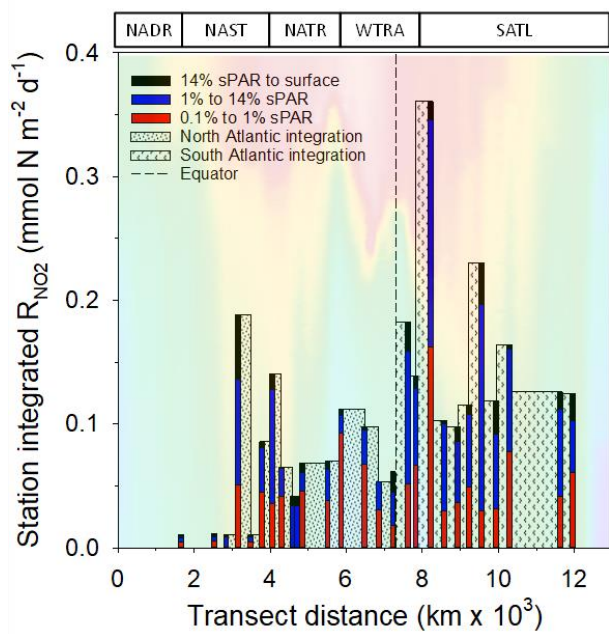
Figure 8. R_{NO2} integrated to the 0.1% sPAR depth at individual stations. These values (excluding stations 28°S and
39°S) are extrapolated between stations extending from the equator to a comparable distance north (33 °N) and south
(35 °S) of the equator. The concentration of ammonium-N oxidised was calculated to be 0.36 mol N d^{-1} over a 1 m x
4457 km distance north of the equator and 0.72 mol N d^{-1} over a 1 m x 4637 km distance south of the equator. Seawater
temperature (as presented in Fig. 2) is included to provide illustrative context to the data. The approximate position of
Longhurst provinces (defined in Fig. 1) is indicated.
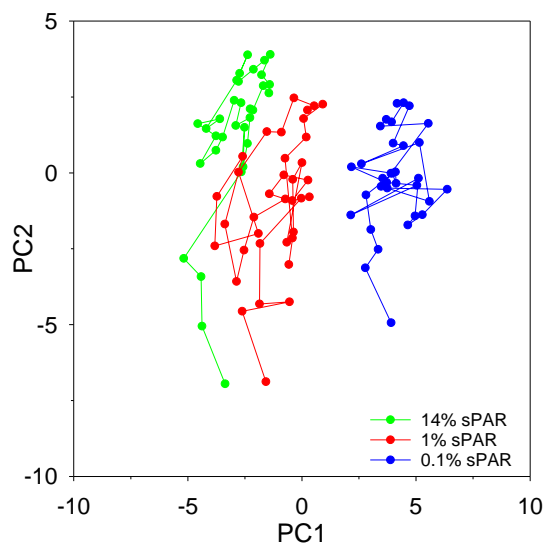
Figure 9. Principle component analysis (PCA) ordination, highlighting the clustering of samples from specific light
equivalent depths. PC1, separating the sPAR bands, explained 42.7% of the total variation while PC2, representing
latitudinal variation, explained 23.4%. In combination, ~65% of variability was explained, leaving ~35% unexplained.
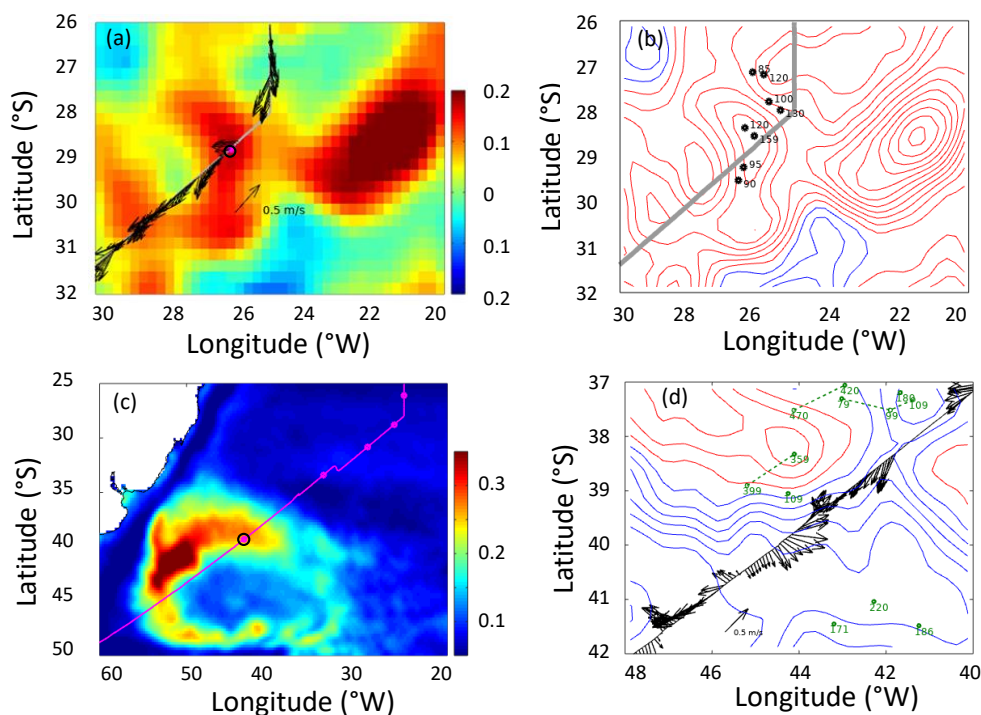
855

860

Figure 10. Altimetry, ship and Argo profiler data relating to the two anomalous stations, indicated by magenta dots
with black boundaries. a) Sea surface height anomaly (SSHA) at the time of the 28°S station. The altimetry shows a
high (anticyclone) centred on the station, with a larger feature further east. The arrows provide the currents at 54 m

865   depth from the shipborne ADCP. b) The same altimetry data as contours (intervals of 0.03 m), with dots indicating
Argo profiles within 5 days of ship passage, and the numbers being the Mixed Layer Depth (depth at which temperature
drops more than 3°C below the surface value. c) The root mean square variability in SSHA showing the pattern of large
signals associated with the Brazil-Falklands Confluence, and the position of the 39°S station. d) Contours of SSH (0.10
m increment, with red for the zero and positive values; blue lines for negative values). The arrows show currents from

870   the shipborne ADCP at 54 m depth, and the dots and green numbers indicate Argo profiles and MLD within 10 days of
ship transit. (Green dashed lines link successive profiles of the same float, with all three being advected eastward).

875

880

Table 1

Results of Principle Components analysis. Eigenvalues are presented in panel (A). In panel (B), Eigenvectors are presented, the coefficients in linear combinations of variables making up principal components (PC).

885   A

PC	Eigenvalues	% Variation	Cum.% Variation
1	9.81	42.7	42.7
2	5.38	23.4	66.1
3	1.64	7.1	73.2
4	1.19	5.2	78.3
5	1.16	5.1	83.4

B

Variable	PC1	PC2	PC3	PC4	PC5
Par (μW cm^{-2})	-0.279	0.097	-0.105	0.143	-0.039
Light (hours)	-0.037	-0.267	-0.449	0.171	0.249
Light (W m^{-2} d^{-1})	-0.28	0.086	-0.123	0.15	-0.03
Conductivity (S m^{-1})	-0.185	0.298	0.118	0.054	0.244
Chlorophyll (mg m^{-3})	-0.056	-0.288	0.258	-0.04	0.332
Dissolved oxygen (μmol L^{-1})	-0.151	-0.076	-0.373	-0.413	-0.379
Salinity	-0.036	0.307	0.152	-0.283	0.164
Temperature (°C)	-0.196	0.279	0.104	0.084	0.26
NO$_2^-$ (μmol L^{-1})	-0.003	-0.252	0.263	-0.466	-0.136
NO$_2^-$ + NO$_3^-$ (μmol L^{-1})	0.259	-0.165	0.162	0.138	-0.034
NO$_3^-$ (μmol L^{-1})	0.244	-0.169	0.223	0.2	-0.103
PO$_4^{3-}$ (μmol L^{-1})	0.203	-0.243	-0.072	0.122	0.266
Si (μmol L^{-1})	0.236	-0.066	0.165	0.254	-0.047
P* (μmol L^{-1})	0.013	-0.221	-0.398	-0.232	0.499
Synechococcus (cell mL^{-1})	-0.255	-0.152	-0.046	0.227	-0.26
Prochlorococcus (cell mL^{-1})	-0.25	0.146	0.206	-0.09	0.166
Pico-eukaryote (<2μm; cell mL^{-1})	-0.231	-0.197	0.24	-0.247	0.067
Nano-eukaryote (2-12μm; cell mL^{-1})	-0.261	-0.2	0.027	0.008	0.075
Coccolithophores (cell mL^{-1})	-0.205	-0.174	0.194	0.149	0.19
Cryptophytes (cell mL^{-1})	-0.089	-0.311	0.191	-0.184	-0.022
Low nucleic acid bacteria (cell mL^{-1})	-0.279	-0.14	0.015	0.158	-0.124
High nucleic acid bacteria (cell mL^{-1})	-0.292	-0.099	0.043	0.187	-0.083
Heterotrophic protists (cell mL^{-1})	-0.239	-0.226	0.057	0.143	-0.107

890